2. EXPLANATORY NOTES[1]

Shipboard Scientific Party[2]

INTRODUCTION

In this chapter, we have assembled information that will help the reader understand the observations on which our preliminary conclusions have been based and also help the interested investigator to select samples for further analysis. This information concerns only shipboard operations and analyses described in the site reports in the *Initial Reports* volume of the Leg 159 *Proceedings of the Ocean Drilling Program.* Methods used by various investigators for shore-based analyses of Leg 159 data will be described in the individual scientific contributions to be published in the *Scientific Results* volume.

Authorship of Site Chapters

The separate sections of the site chapters were written by the following shipboard scientists (names are listed in alphabetical order; no seniority is implied):

Site Summary: G.P. Lohmann, Jean Mascle
Background and Objectives: G.P. Lohmann, Jean Mascle
Operations: Peter Clift, Mike Storms
Site Geophysics: Rosemary Edwards, Jean Mascle
Lithostratigraphy: Emmanuel Brantuoh, Peter Clift, Kenichiro Hisada, Mary Anne Holmes, Kyger C Lohmann, Francisca Oboh, Thomas Pletsch, Kari Strand
Biostratigraphy: Jean-Pierre Bellier, Richard Norris, Samir Shafik, Im Chul Shin, David Watkins
Sedimentation Rates: David Watkins
Paleomagnetism: Simon Allerton, Carlos Mortera-Gutierrez
Organic Geochemistry: Eric Barton, Thomas Wagner
Structural Geology: Jean Benkhelil, Elizabeth Pickett
Inorganic Geochemistry: Enriqueta Barrera, Greg Ravizza
Source Rock Geochemistry: Eric Barton
Physical Properties: Thomas Akamaluk, Maria Ask, Aleksandra Janik, Sumito Morita
Downhole Measurements: Christophe Basile, Eileen Ewert, Carlos Gonçalves

Summary core descriptions ("barrel sheets") and photographs of each core are included in a section called "Cores" following the text of all site chapters.

Drilling Characteristics

Because water circulation through the drill pipe is an open system, cuttings are lost onto the seafloor and cannot be examined. The properties of the uncored or unrecovered intervals may be inferred from seismic data, from wireline-logging results, and from an examination of the behavior of the drill string, as observed and recorded on the drilling platform. Typically, the harder a layer, the slower and more difficult it is to penetrate. A number of other factors may determine the rate of penetration, thus, it is not always possible to relate drilling time directly to the hardness of the layers. Bit weight and revolutions per minute, recorded on the drilling recorder, also influence penetration rate.

Drilling Disturbance

When split, many cores show signs of significant sediment disturbance, including the concave-downward appearance of originally horizontal bands, haphazard mixing of lumps of different lithologies (mainly at the tops of cores), and the near-fluid state of some sediments recovered from tens to hundreds of meters below the seafloor. Core deformation probably occurs during cutting, retrieval (with accompanying changes in pressure and temperature), and core handling on deck.

Shipboard Scientific Procedures

Numbering of Sites, Holes, Cores, and Samples

Ocean Drilling Program (ODP) drill sites are numbered consecutively and refer to one or more holes drilled while the ship was positioned over one acoustic beacon. Multiple holes may be drilled at a single site by pulling the drill pipe above the seafloor (out of the hole), moving the ship some distance from the previous hole, and then drilling another hole.

For all ODP drill sites, a letter suffix distinguishes holes drilled at the same site. For example, the first hole to be drilled is assigned the site number modified by the suffix *A,* the second hole takes the site number and suffix *B,* and so forth. Note that this procedure differs slightly from that used by the Deep Sea Drilling Project (DSDP; Sites 1 through 624), but prevents ambiguity between site- and hole-number designations. It is important to distinguish among holes drilled at a site, because recovered sediments or rocks from different holes usually do not come from equivalent positions in the stratigraphic column.

The cored interval is measured in meters below seafloor (mbsf). The depth interval assigned to an individual core begins with the depth below the seafloor at which the coring began, and extends to the depth at which coring ended. For example, each coring interval is generally up to 9.5 m long, which is the length of a core barrel. Coring intervals may be shorter and may not necessarily be adjacent if separated by drilled intervals. In soft sediments, the drill string can be "washed ahead" with the core barrel in place, without recovering sediments. This is achieved by pumping water down the pipe at high pressure to wash the sediment out of the way of the bit and up the space between the drill pipe and the wall of the hole. If thin, hard, rock layers are present, then it is possible to get "spotty" sampling of these resistant layers within the washed interval, and thus to have a cored interval greater than 9.5 m.

Cores taken from a hole are numbered serially from the top of the hole downward. Core numbers and their associated cored intervals in meters below seafloor usually are unique in a given hole; however, this may not be true if an interval must be cored twice, because of caving of cuttings or other hole problems. Maximum recovery for a

[1]Mascle, J., Lohmann, G.P., Clift, P.D., et al., 1996, *Proc. ODP, Init. Repts.,* 159: College Station, TX (Ocean Drilling Program).
[2]Shipboard Scientific Party is given in the list preceding the Table of Contents.

single core is 9.5 m of rock or sediment contained in a plastic liner (6.6 cm internal diameter) plus about 0.2 m (without a plastic liner) in the core catcher (Fig. 1). The core catcher is a device at the bottom of the core barrel that prevents the core from sliding out when the barrel is being retrieved from the hole.

A recovered core is divided into 1.5-m sections that are numbered serially from the top (Fig. 1). When full recovery is obtained, the sections are numbered from 1 through 7, with the last section possibly being shorter than 1.5 m (rarely, an unusually long core may require more than seven sections). When less than full recovery is obtained, as many sections as needed to accommodate the length of the core will be recovered; for example, 4 m of core would be divided into two 1.5-m sections and one 1-m section. If cores are fragmented (recovery less than 100%), sections are numbered serially and intervening sections are noted as void, whether or not shipboard scientists think that the fragments were contiguously in situ. In rare cases, a section less than 1.5 m may be cut to preserve features of interest (e.g., lithologic contacts).

By convention, material recovered from the core catcher is placed below the last section when the core is described and is labeled core catcher (CC); in sedimentary cores, this is treated as a separate section. The core catcher is placed at the top of the cored interval in cases where material is recovered only in the core catcher. However, information supplied by the drillers or by other sources may allow for more precise interpretation as to the correct position of core-catcher material within an incompletely recovered cored interval.

When the recovered core is shorter than the cored interval, the top of the core is equated with the top of the cored interval by convention to achieve consistency when handling analytical data derived from the cores. Samples removed from the cores are designated by distance measured in centimeters from the top of the section to the top and bottom of each sample removed from that section.

A complete identification number for a sample consists of the following information: leg, site, hole, core number, core type, section number, piece number (for hard rock), and interval in centimeters measured from the top of the section. For example, a sample identification of "159-959B-25R-1, 10–12 cm" would correspond to a sample removed from the interval between 10 and 12 cm below the top of Section 1, Core 25 (R designates that this core was taken during rotary drilling) of Hole 959B during Leg 159.

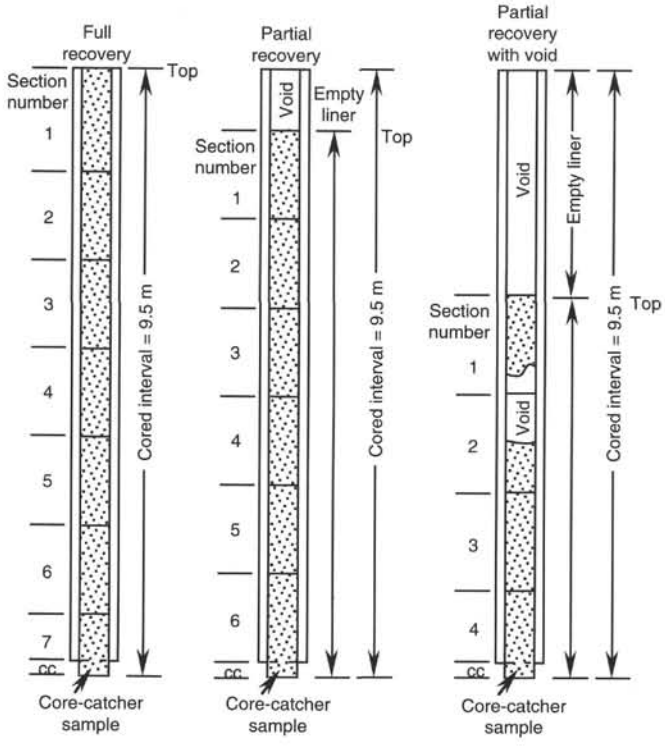

Figure 1. Examples of numbered core sections.

All ODP core and sample identifiers indicate core type. The following abbreviations were used: R = rotary core barrel (RCB); H = hydraulic piston core (HPC; also referred to as APC, or advanced hydraulic piston core); P = pressure core barrel; X = extended core barrel (XCB); B = drill-bit recovery; C = center-bit recovery; I = in situ water sample; S = sidewall sample; W = washed-core recovery; and M = miscellaneous material. APC, XCB, and RCB cores were cut during Leg 159.

Core Handling

Sediments

As soon as a core is retrieved on deck, a sample is taken from the core catcher and given to the paleontology laboratory for an initial age assessment. Then, the core is placed on a long horizontal rack, and gas samples may be taken by piercing the core liner and withdrawing gas into a vacuum tube. Voids within the core are sought as sites for gas sampling. Some of the gas samples are stored for shore-based study; however, others are analyzed immediately as part of the shipboard safety and pollution-prevention program. Next, the core is marked into section lengths, each section is labeled, and the core is cut into sections. Interstitial-water and physical properties samples then are taken. In addition, headspace gas samples are scraped routinely from the end of one cut section from each core on the catwalk and sealed in glass vials for light hydrocarbon analysis. Each section then is sealed at the top and bottom by gluing on color-coded plastic caps, blue to identify the top of a section and clear to identify the bottom. A yellow cap is placed on the section ends from which a whole-round sample has been removed. These caps are usually attached to the liner by coating the end liner and the inside rim of the cap with acetone, and then the caps are taped to the liners.

Next, the cores are carried into the laboratory, where the sections again are labeled, using an engraver to mark the full designation of the section permanently. The lengths of the core in each section and the core-catcher sample are measured to the nearest centimeter; this information is logged into the shipboard CORELOG database program. Whole-round sections from APC and XCB cores normally are run through the multisensor track (MST). The MST includes the gamma-ray attenuation porosity evaluator (GRAPE) and *P*-wave logger devices, which measure bulk density, porosity, and sonic velocity, and also includes a meter that determines volume magnetic susceptibility. After the core has equilibrated to room temperature (approximately 3 hr), thermal conductivity measurements are performed on relatively soft sediments, and the cores are split.

Cores of soft material are split lengthwise into working and archive halves. The softer cores are split with a wire or saw, depending on the degree of induration. Harder cores are split with a band saw or diamond saw. During Leg 159, the wire-cut cores were split from the bottom to top; thus, investigators should be aware that older material may have been transported up the core on the split face of each section.

The working half of the core is sampled for both shipboard and shore-based laboratory studies. Each extracted sample is logged into the sampling computer database program by the location and the name of the investigator receiving the sample. Records of all removed samples are kept by the curator at ODP. The extracted samples are sealed in plastic vials or bags and labeled. Samples are routinely taken for shipboard physical properties analysis. These samples subsequently are used for calcium carbonate (coulometric analysis) and organic carbon (CNS elemental analyzer) analyses, and these data are reported in the site chapters.

The archive half is described visually. Smear slides are made from samples taken from the archive half and are supplemented by thin sections taken from the working half. Most archive sections are run

through the cryogenic magnetometer. The archive half then is photographed, a whole core at a time, using both black-and-white and color film. Close-up photographs (black-and-white) are taken of particular features for illustrations in the summary of each site, as requested by individual scientists.

Both halves of the core then are placed into labeled plastic tubes, sealed, and transferred to cold-storage space aboard the drilling vessel. At the end of Leg 159, the cores were transferred from the ship in refrigerated airfreight containers to cold storage at the Bremen Core Repository of the Ocean Drilling Program, at the University of Bremen, Federal Republic of Germany.

Indurated Sedimentary Rocks

Low-recovery cores containing indurated sedimentary rock were handled differently from less lithified cores. Once on deck, the core-catcher sample is placed at the bottom of the core liner and total core recovery is calculated by shunting the rock pieces together and measuring to the nearest centimeter, this information is logged into the shipboard CORELOG database program. The core then is cut into 1.5-m-long sections and transferred into the laboratory.

The contents of each section are transferred into 1.5-m-long sections of split core liner, where the bottom of oriented pieces (i.e., pieces that clearly could not have rotated top to bottom about a horizontal axis in the liner) are marked with a red wax pencil. This is to ensure that orientation is not lost during the splitting and labeling processes. Because pieces are free to turn about a vertical axis during drilling, azimuthal orientation during Leg 159 was possible only by using paleomagnetic or downhole logging data and could not be recorded at this time. Important primary features of the cores also are recorded at this time. The core then is split into archive and working halves. A plastic spacer is used to separate individual pieces and/or reconstructed groups of pieces in the core liner. These spacers may represent a substantial interval of no recovery.

In splitting the core, every effort is made to ensure that important features are represented in both halves. The working half is sampled for shipboard physical properties measurements, magnetic studies, X-ray fluorescence (XRF), X-ray diffraction (XRD), and thin-section studies. Nondestructive physical properties measurements, such as magnetic susceptibility, are performed on the archive half of the core. Where recovery permits, samples are taken from each lithologic unit. Some of these samples are minicores. The archive half is described using the visual core description (VCD) form and is photographed before storage.

The working half of the hard-rock core then is sampled for shipboard laboratory studies. Records of all samples are kept by the curator at ODP. The archive half is described visually, then photographed with both black-and-white and color film, one core at a time. Both halves of the core then are shrink-wrapped in plastic to prevent rock pieces from vibrating out of sequence during transit, placed into labeled plastic tubes, sealed, and transferred to cold-storage space aboard the drilling vessel. As with the other Leg 159 cores, they are housed at the Bremen Core Repository.

LITHOSTRATIGRAPHY

Sediment Core Description

Core Description Forms and the "VCD" Program

The core description forms (Fig. 2), or "barrel sheets," summarize the data obtained during shipboard analysis of each sediment core. During Leg 159 these were generated using the ODP in-house Macintosh application "VCD" (edition 1.0.Op1, customized for this leg). The following discussion explains the ODP conventions used in compiling each part of the core description forms, the use of "VCD" to generate these forms, and the exceptions to these procedures adopted by the Leg 159 shipboard party.

Shipboard sedimentologists were responsible for visual core logging, smear slide analyses, and thin-section descriptions of sedimentary material. Core descriptions were initially recorded by hand on a section-by-section basis on standard ODP Visual Core Description forms (VCD forms, not to be confused with the "VCD" Macintosh application). Use of these forms is now considered optional by ODP, and on some recent legs visual description was carried out directly at the core-by-core level using the "VCD" application. During Leg 159, however, we considered it desirable to preserve fine-detail observations that are lost at the core-by-core "barrel sheet" level. Structural geologists also recorded structures on VCD forms of their own design (Fig. 3). The Visual Core Description forms are available from ODP on request.

For each hole a Master Column was prepared (Fig. 4). This form indicates recovery, summarizes the lithology, and charts a variety of data against sub-bottom depth (e.g., biostratigraphic zones, magnetochrons, structural geology, chemistry, physical properties, and logging). The Master Columns supplement the information contained on the core description forms at a further condensed scale.

Core Designation

Cores are designated using leg, site, hole, core number, and core type as discussed previously in the "Numbering of Sites, Holes, Cores, and Samples" section. The cored interval is specified in meters below seafloor (mbsf). On the basis of drill-pipe measurements (dpm), reported by the SEDCO coring technician and the ODP operations manager, depths are corrected for the height of the rig-floor dual elevator stool above sea level to give true water depth and correct mbsf.

Graphic Lithology Column

The lithology of the material recovered is represented on the core description forms (Fig. 2) by up to three symbols within a single depth interval (Fig. 5) in the column titled "Graphic Lithology." Relative abundance of each lithology is indicated by the column width, with the most abundant lithology in the right-most column. Where an interval of sediment or sedimentary rock is a homogeneous mixture of lithologies, the constituent categories are separated by solid vertical lines, with each category represented by its own symbol. Constituents accounting for <10% of the sediment in a given lithology (or others remaining after the representation of the three most abundant lithologies) are not shown in the graphic lithology column but are listed in the "Lithologic Description" section of the core description form. In an interval comprising two or more interbedded sediment lithologies that have quite different compositions, such as in thin-bedded and highly variegated sediments, the average relative abundances of the lithologic constituents are represented graphically by dashed lines that vertically divide the interval into appropriate fractions, as described above. Because the graphic lithology column shows only the composition of layers or intervals exceeding 20 cm in thickness, important sedimentary features present at intervals less than 20 cm thick are illustrated in the sedimentary structures column.

Age Column

The chronostratigraphic unit, as recognized on the basis of paleontological and paleomagnetic criteria, is shown in the "Age" column on the core description forms (Fig. 2). Boundaries between assigned ages are indicated as follows:

1. Sharp boundary: straight line;

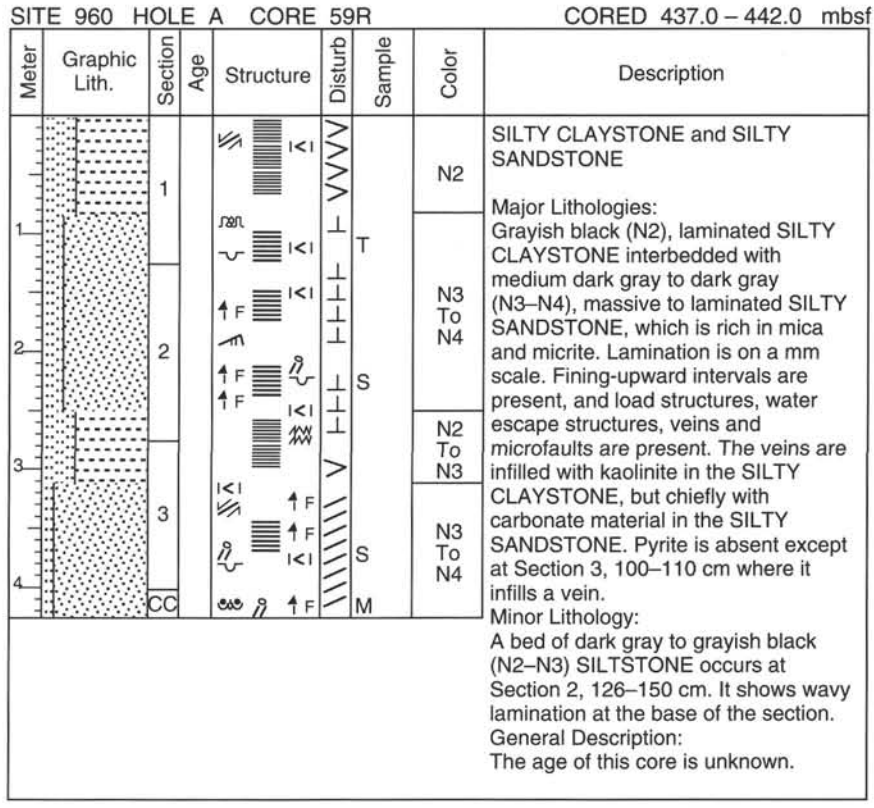

Figure 2. Example of core description form ("barrel sheet") used for sediments and sedimentary rocks.

2. Unconformity or hiatus: line with + signs above it;
3. Uncertain: line with question marks.

Sedimentary Structures

In sediment cores, natural structures are indicated in the "Structure" column of the core description forms (Fig. 2). The column is divided into three vertical areas for symbols. These include features related to sedimentary bedding, transport/erosion, bed contacts, bioturbation intensity, as well as syn-depositional and post-depositional deformation. The symbols used to describe each of these primary and secondary biogenic and physical sedimentary structures are shown in Figure 6. Only structures definitely distinguished from coring induced features are illustrated.

Sediment Disturbance

Sediment disturbance resulting from the coring process is illustrated in the "Disturbance" column on the core description forms (using symbols in the right column of Fig. 6). Blank regions indicate a lack of drilling disturbance. The degree of drilling disturbance is described for soft and hard sediments using the following categories:

1. Slightly deformed: bedding contacts are slightly bent.
2. Moderately deformed: bedding contacts have undergone extreme bowing.
3. Highly deformed: bedding is completely disturbed, sometimes showing symmetrical diapir-like or flow structures.
4. Soupy: intervals are water saturated and have lost all aspects of original bedding.

The degree of fracturing in indurated sediments and rock is described using the following categories:

1. Slightly fractured: core pieces are in place and contain little drilling slurry or breccia.
2. Moderately fragmented: core pieces are in place or partly displaced, but original orientation is preserved or recognizable (drilling slurry may surround fragments).
3. Highly fragmented: core pieces are from the interval cored and probably are in correct stratigraphic sequence (although they may not represent the entire section), but original orientation is completely lost.
4. Drilling breccia: core pieces have lost their original orientation and stratigraphic position and may be mixed with drilling slurry.

Color

The hue and chroma attributes of color, determined using Munsell Soil Color Charts (1975), were measured as soon as possible after the cores were split and covered with plastic wrap, because redox-associated color changes may occur when deep-sea sediments are exposed to the atmosphere. Core color, rounded to the nearest standard Munsell color value, is given in the "Color" column on the core description form.

Samples

The position of samples taken from each core for shipboard analysis is indicated in the "Samples" column on the core description form, as follows:

S: smear slide;
T: thin section;
P: physical properties sample;
M: micropaleontology sample;
X: paleomagnetic sample;
I: interstitial water sample;
C: organic geochemistry sample;
D: XRD sample;
F: XRF sample.

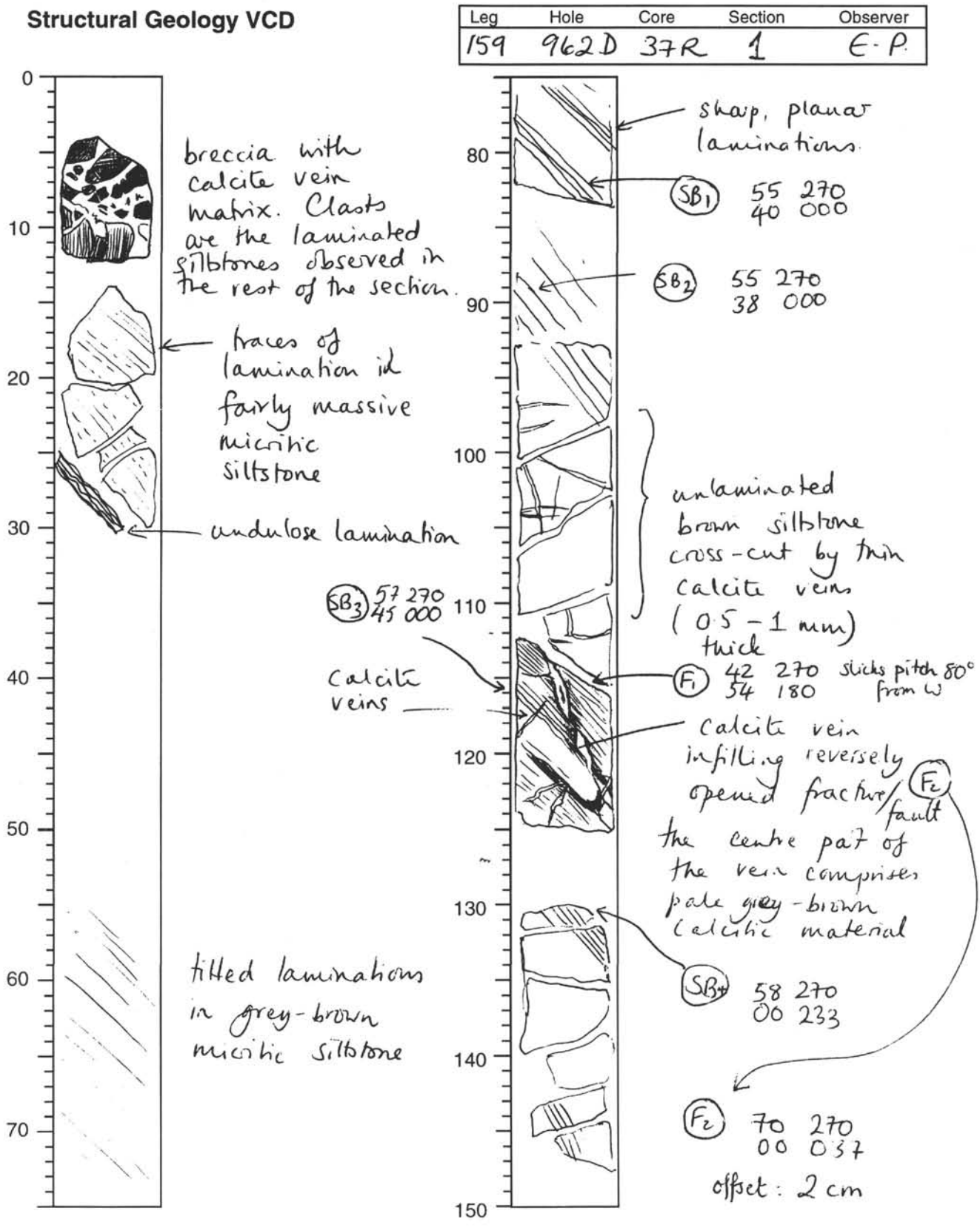

Figure 3. Example of a structural visual core description form (VCD). Vertical scale is in centimeters below the top of the cored interval.

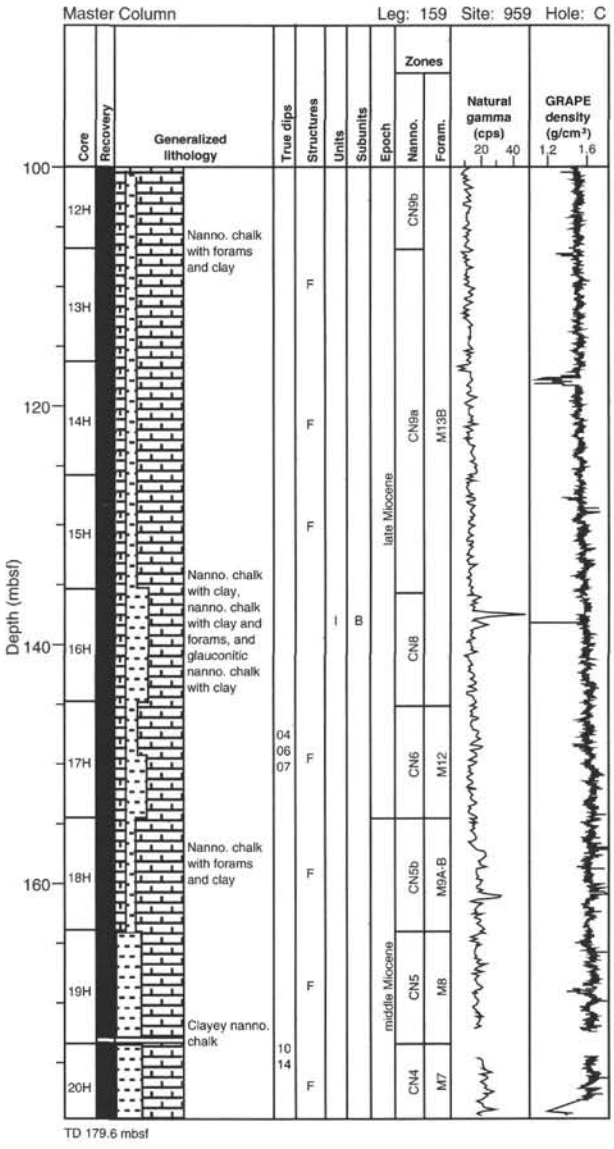

Figure 4. Example of a hole Master Column.

Lithologic Description-Text

The lithologic description that appears on each core description form consists of three parts: (1) a heading that lists all the major sediment lithologies observed in the core; (2) a heading for minor lithologies, and (3) a more detailed description of these sediments, including features such as color, composition (determined from the analysis of smear slides), sedimentary structures, or other notable characteristics. Descriptions and locations of thin, interbedded, or minor lithologies, which cannot be depicted in the graphic lithology column provided by the VCD program, are included in the text.

Smear Slide and Thin-section Summary

All biotic and abiotic components identified from smear slides and thin sections are summarized on the stratigraphic log provided as specified within each site chapter in the "Smear Slides" section in the back of this volume. This table includes information on the sample location, whether the sample represents a dominant ("D") or a minor ("M") lithology in the core, and the estimated percentages of all identified components.

SEDIMENT CLASSIFICATIONS

Classification of Sediments and Sedimentary Rocks

Leg 159 used a modified version of the sediment classification scheme of the Ocean Drilling Program (Shipboard Scientific Party, 1990; Mazzullo et al., 1988) for granular sediment types (Fig. 7). Variations in the relative proportions of pelagic, siliciclastic, neritic, and volcaniclastic grain types define five major classes of granular sediments. Pelagic grains are the skeletal remains of open-marine siliceous and calcareous microfauna and microflora (e.g., radiolarians, diatoms, planktonic foraminifers, nannofossils) and associated organisms. Siliciclastic grains are mineral and rock fragments derived from igneous (plutonic and volcanic), sedimentary, and metamorphic rocks. Neritic grains include allochemical components (e.g., ooliths, pisoliths), the skeletal remains of shallow marine flora and fauna (e.g., bioclasts), or aggregate grains comprising fine- to coarse-grained sediment (e.g., peloids, intraclasts). Volcaniclastic grains include those of pyroclastic origin (direct products of magma degassing or water/magma interaction) and epiclastic origin (detritus derived from erosion of volcanic rocks).

A granular sediment is classified by designating a principal name and major and minor modifiers. The principal name of a granular sediment defines its granular-sediment class; the major and minor modifiers describe the texture, composition, and fabric.

Principal Names

For siliciclastic sediment, the principal name describes the texture and is assigned according to the following guidelines:

1. The Udden-Wentworth grain-size scale (Wentworth, 1922; Fig. 8) defines grain-size ranges and names of the textural groups (gravel, sand, silt, and clay) and subgroups (fine sand, coarse silt, etc.) that are used as the principal names of siliciclastic sediment.
2. Principal names are listed in order of increasing abundance when two or more textural groups or subgroups are present in a siliciclastic sediment (Shepard, 1954; Fig. 9).
3. The suffix "-stone" is affixed to the principal names sand, silt, and clay when the sediment is lithified. Conglomerate and breccia are used as principal names of lithified gravels with well-rounded and angular clasts, respectively.

For pelagic sediment, the principal name describes the composition and degree of consolidation using the following terms:

1. Ooze: unlithified calcareous and/or siliceous pelagic sediments;
2. Chalk: partially lithified pelagic sediment predominantly composed of calcareous pelagic grains;
3. Limestone: lithified pelagic or neritic sediment predominantly composed of calcareous grains; and
4. Radiolarite and diatomite: partially lithified pelagic sediment predominantly composed of siliceous radiolarians, or diatoms, respectively.
5. Porcellanite and chert: partially lithified and lithified biosiliceous sediments, respectively.

Major and Minor Modifiers

The principal name of a granular-sediment class is preceded by major modifiers and followed by minor modifiers (preceded by "with") that describe the lithology of the granular sediment in greater detail. Major and minor modifiers are used most commonly to describe composition and textures of grain types present in major (>25%) and minor (10%–25%) proportions and to describe grain fabric (e.g., matrix supported).

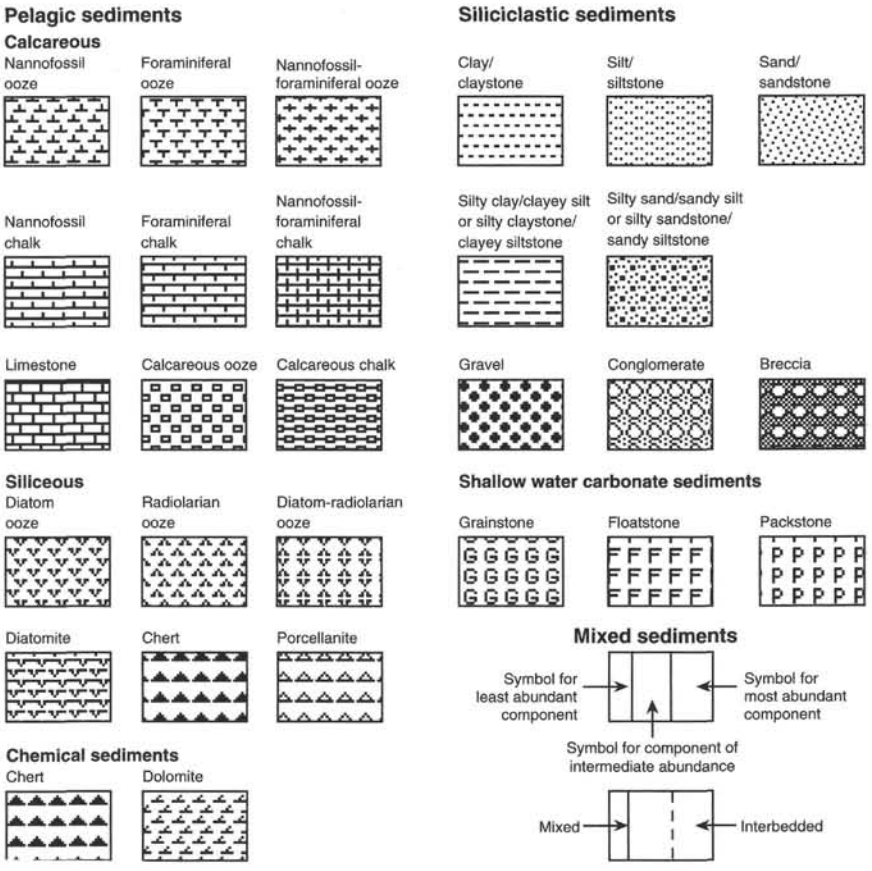

Figure 5. Key to symbols used in the "graphic lithology" column on the core description form shown in Figure 2.

The composition of pelagic grains can be described with the major and minor modifiers diatom(-aceous), radiolarian, spicule(-ar), siliceous, nannofossil, foraminifer(-al), and calcareous. The terms siliceous and calcareous are used generally to describe sediments composed of siliceous or calcareous pelagic grains of mixed origins. Sediment fabric can be described by the major modifiers grain-supported or matrix-supported. Generally, fabric descriptors are applied only to gravels, conglomerates, and breccias.

The degree of consolidation is described using the following major modifiers: "unlithified" designates soft sediment that is readily deformable under the pressure of a finger, "partially lithified" designates firm sediment that is incompletely lithified, and "lithified" designates hard, cemented sediment that must be cut with a saw.

Grain shapes are described by the major modifiers rounded, subrounded, subangular, and angular. Sediment color can be employed as a major modifier.

Mixed sediments are described using major and minor modifiers indicating composition and texture.

X-ray Diffraction Methods for Bulk Mineralogic Determinations

Selected samples were taken for analysis by X-ray diffraction (XRD) using a Philips APD 3720, operated by Philips software PCAPD v. 3.0. The diffractometer was operated using CuK-alpha radiation, at 35 mA and 40 kV, with a focusing graphite monochromator and a 12.5-mm theta compensating slit. Samples analyzed as bulk samples were freeze-dried, ground with an agate mortar and pestle, and packed in sample holders, imparting some orientation to the clay minerals. These were scanned from 2° to 70° 2θ. Other samples were analyzed for clay mineral determination, and these were not freeze-dried nor ground, but mixed with a 1% calgon solution and ultrasonicated for up to 10 min with a Fisher Sonic Dismembrator. If this did not effect deflocculation, the supernatant was decanted and more calgon was added until the clays remained deflocculated for more than 1 hr. After 1 hr of settling, an aliquot of the suspension was drawn off from a 1-cm water depth using a pipette and put into a Milipore filtration apparatus with a 0.45-µm membrane filter. The clay cake was transferred from the membrane filter to a glass slide by placing the filter on the slide and rolling the paper with a small glass beaker. When air dried, clay samples were scanned from 2° to 70° 2θ, then placed over ethylene glycol in a desiccator at room temperature for 24 hr, and scanned again from 2° to 35° 2θ. The samples were then heated to 550°C for 1 hr, and scanned again from 2° to 35° 2θ.

Mineral identification followed more or less standard procedures as outlined in Moore and Reynolds (1989), Brown and Brindley (1980), and Brown (1980). Selected diffractograms illustrating which peaks we associated with various minerals are given in the various site chapters.

BIOSTRATIGRAPHY

Preliminary age determinations for Leg 159 sediments are based on biostratigraphic analysis of calcareous nannofossils and planktonic foraminifers. Stratigraphic estimates of both nannofossil and planktonic foraminiferal datums were based on examination of one to six samples per core, with a sample spacing of 1.5 to 9.5 m. If more than one APC hole was cored at one site (as was the case at Site 959), we adopted the sampling strategy used on Leg 138 (Mayer, Pisias,

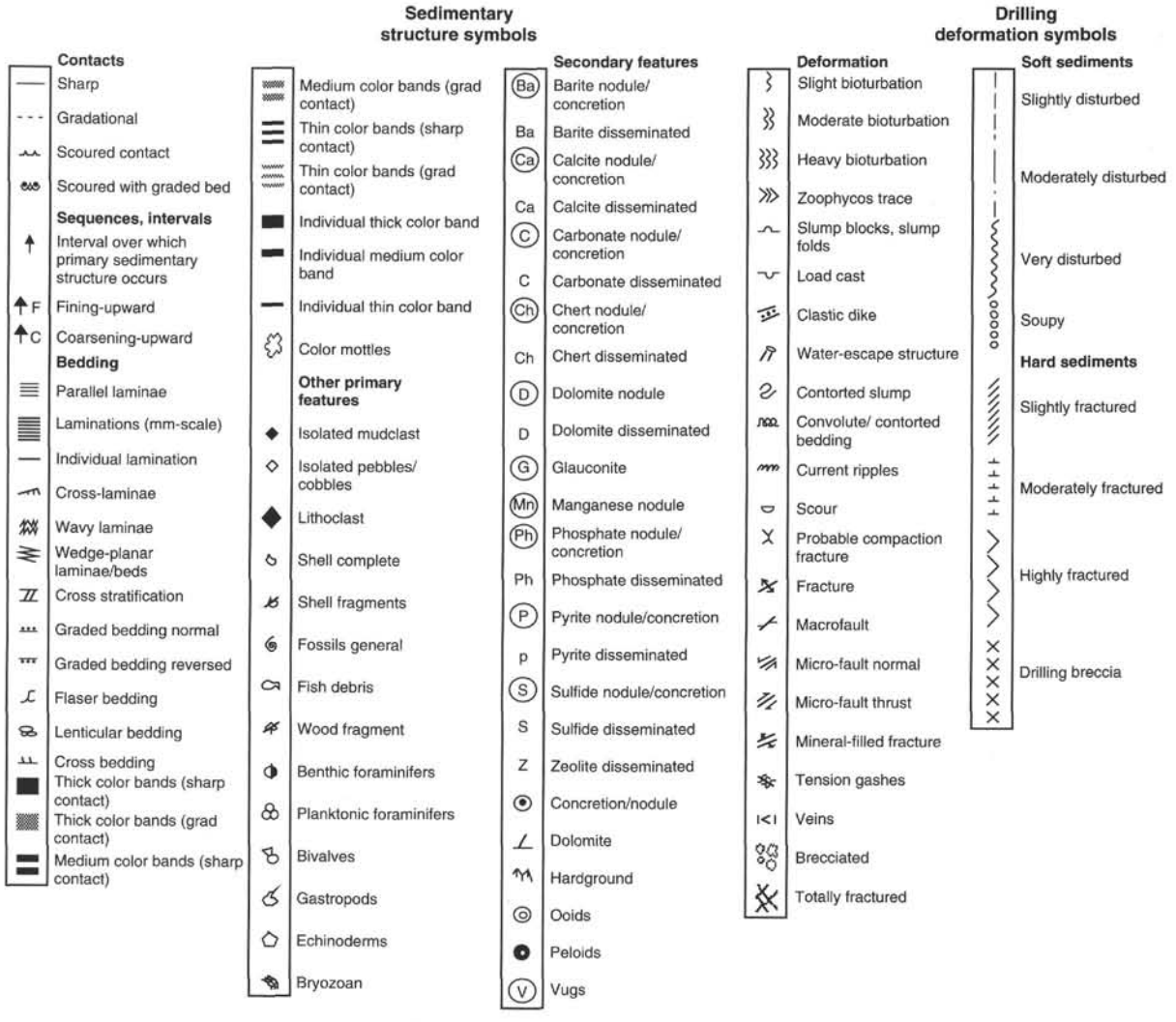

Figure 6. Symbols used for drilling disturbance and sedimentary structure on core description forms shown in Figure 2.

Janecek, et al., 1992) and Leg 154 (Curry, Shackleton, Richter, et al., 1995) of concentrating our efforts on a single APC hole and correlating to adjacent holes using assemblages in core catchers.

Sample positions and the abundance, preservation, and chronostratigraphic age or biozone for calcareous nannofossils, planktonic foraminifers, and benthic foraminifers were recorded on core description forms for each core. The geochronologic time scale of Cande and Kent (1992) is used for the Cenozoic and Late Cretaceous. The Early Cretaceous geochronology is based on Harland et al. (1990). Figure 10 shows the correlations among Cenozoic calcareous nannofossil and planktonic foraminifer biozones and the geomagnetic polarity time scale used during Leg 159. Figure 11 shows the correlation chart for the Cretaceous.

Calcareous Nannofossils

Zonation

For most of the Cenozoic assemblages, we used the zonation of Okada and Bukry (1980). This zonation, based originally on low-latitude oceanic assemblages (Bukry, 1973, 1975), is thought more suited to Leg 159 material than the mid-latitude, land-based zonation of Martini (1971). However, some of Martini's (1971) zonal and subzonal indicators were used where feasible, as intrazonal biohorizons, to improve stratigraphic resolution.

We followed the high-resolution zonation proposed by Gartner (1977) and Rio et al. (1990) for the Quaternary.

For the Cretaceous assemblages, we used the zonation of Sissingh (1977) augmented by additional biohorizons from Perch-Nielsen (1985) with reference to Thierstein (1973, 1976), and Roth (1978). The sequence of biohorizons, and their chronostratigraphic correlations, follow the scheme of Erba et al. (in press).

Methods

Calcareous nannofossil assemblages were analyzed in smear slides prepared from raw sediment samples. Gravitational settling was also used, in a few cases, to concentrate sparse nannofossil assemblages in critical intervals. Slides were examined with the light microscope at 1250× magnification. Estimates for the total nannofossil abundance were determined as follows:

D (dominant): >60% of all particles;
A (abundant): 30%–60% of all particles;
C (common): 10%–30% of all particles;
F (few): 5%–10% of all particles;
R (rare): 1%–5% of all particles;
T (trace): 0.1%–1.0% of all particles;
P (present): <0.1% of all particles;
B (barren): no nannofossils present.

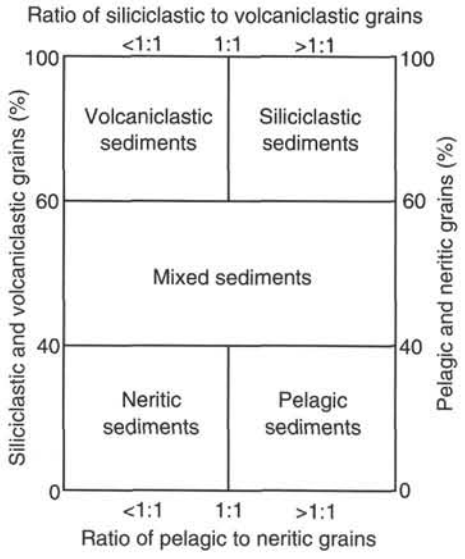

Figure 7. Diagram showing classes of granular sediment (modified from Mazzullo et al., 1988).

Millimeters (mm)	Micrometers (μm)	Phi (ϕ)	Wentworth size class	
4096		−12.0		
256		−8.0	Boulder	
84		−6.0	Cobble	Gravel
4		−2.0	Pebble	
2.00		−1.0	Granule	
1.00		0.0	Very coarse sand	
1/2 — 0.50	— 500	— 1.0	Coarse sand	
1/4 — 0.25	— 250	— 2.0	Medium sand	Sand
1/8 — 0.125	— 125	— 3.0	Fine sand	
1/16 — 0.0625	— 63	— 4.0	Very fine sand	
1/32 — 0.031	— 31	— 5.0	Coarse silt	
1/64 0.0156	15.6	6.0	Medium silt	
1/128 0.0078	7.8	7.0	Fine silt	Mud
1/256 — 0.0039	— 3.9	— 8.0	Very fine silt	
0.00006	0.06	14.0	Clay	

Figure 8. Udden-Wentworth grain-size scale for siliciclastic sediments (Wentworth, 1922).

Estimates of nannofossil preservation are coded as follows:

P (poor): strong overgrowth and dissolution, most specimens fragmented and difficult to identify;
M (moderate): moderate dissolution and overgrowth, most specimens readily identifiable;
G (good): slight dissolution and overgrowth, all taxa easily identifiable;
E (Excellent): pristine preservation with no overgrowth or dissolution.

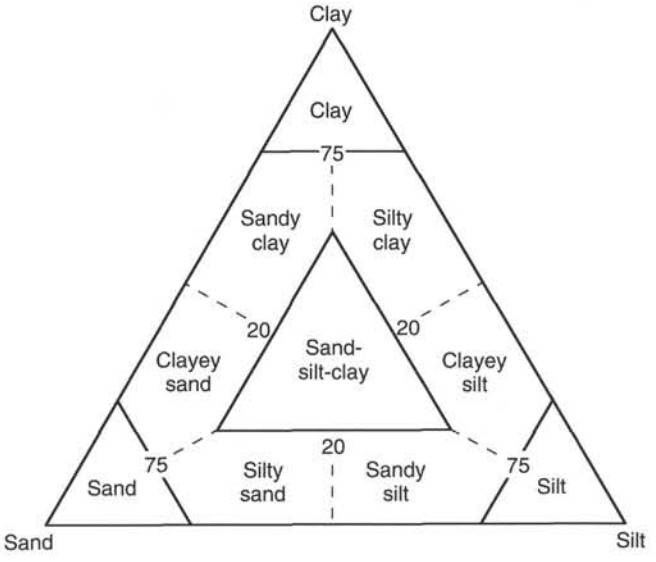

Figure 9. Ternary diagram showing principal names for siliciclastic sediments (modified from Shepard, 1954).

Estimates of the relative abundances of calcareous nannofossil species were determined as follows:

D (dominant): >60% of all nannofossils;
A (abundant): 30%–60% of all nannofossils;
C (common): 10%–30% of all nannofossils;
F (few): 5%–10% of all nannofossils;
R (rare): 1%–5% of all nannofossils;
T (trace): <1% of all particles.

Planktonic Foraminifers

Zonation

The low and middle latitude zonations of Berggren et al. (in press) have been applied to Paleogene and Neogene assemblages (Fig. 10). For the Cretaceous assemblages (Fig. 11), we used the zonal scheme of Caron (1985), which is based partly on the schemes proposed by Robaszynski et al. (1979) and of Robaszynski et al. (1984).

Methods

Samples of about 10 cm^3 from the core catchers and/or taken from the cores were washed directly through 63-μm sieves with tap water or, when more lithified, were soaked in diluted hydrogen peroxide and then washed under running water through 63-μm mesh sieves. Hard lumps were gently crushed between fingers or rubbed over the screen. Methyl Blue was applied to all sieves after washing to stain any foraminifers that might contaminate samples washed at a later time. The 45-μm and 38-μm mesh sieves were used to retain small specimens such as those typical of the early Paleocene as well as species such as pseudohastigerinids, tenuitellids, and chiloguembelinids. Sieved samples were dried in an oven at 80°C and examined under a binocular microscope. Both 250-μm and 150-μm mesh sieve fractions were examined in each sample.

The abundance of single species within the assemblages in the residues was recorded as:

VA = very abundant (>60% of the total fauna);
A = abundant (40%–60%);
F = frequent (40%–20%);
C = common (20%–5%);
R = rare (<5%).

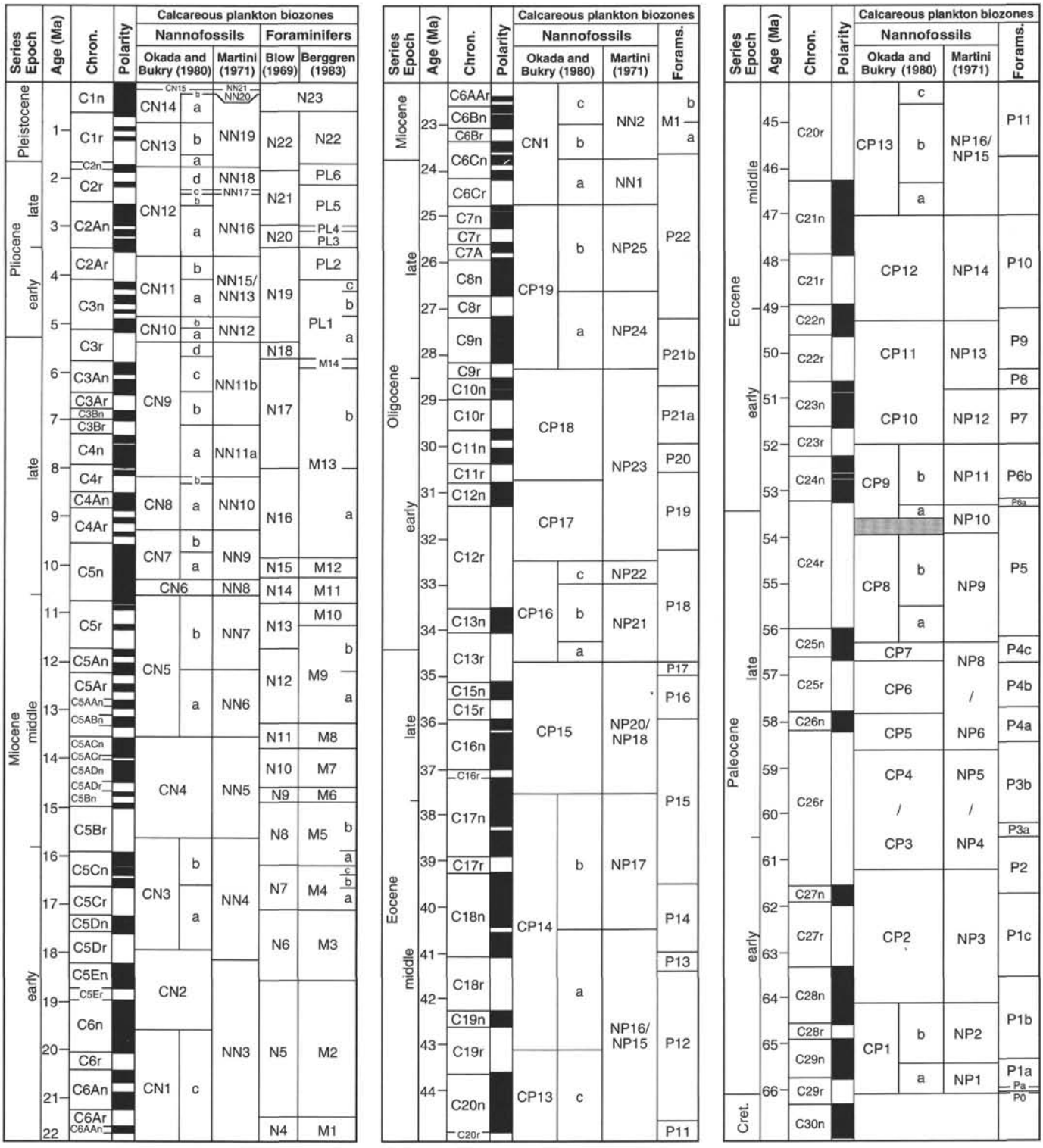

Figure 10. Correlation of Cenozoic nannofossil and planktonic foraminifer zones/subzones with the geomagnetic polarity time scale of Cande and Kent (1992) (modified from Curry et al., 1995, with planktonic foraminifer zonation of Berggren et al., in press).

Preservation includes the effect of diagenesis, abrasion, recrystallization, encrustation, filling with cement and/or dissolution of planktonic foraminifer tests. The degree of preservation of tests is expressed as follows:

E = excellent (no dissolution or breakage, glassy walls)

G = good (no or few dissolution effects are observable, opaque walls, <10% broken specimens, open chamber interiors)

M = moderate (minor but common dissolution, specimens are still recognizable, fragmentation of 10%–70% of specimens, specimens may be filled with cement)

P = poor (strong dissolution affects the assemblages with >70% dissolved or broken).

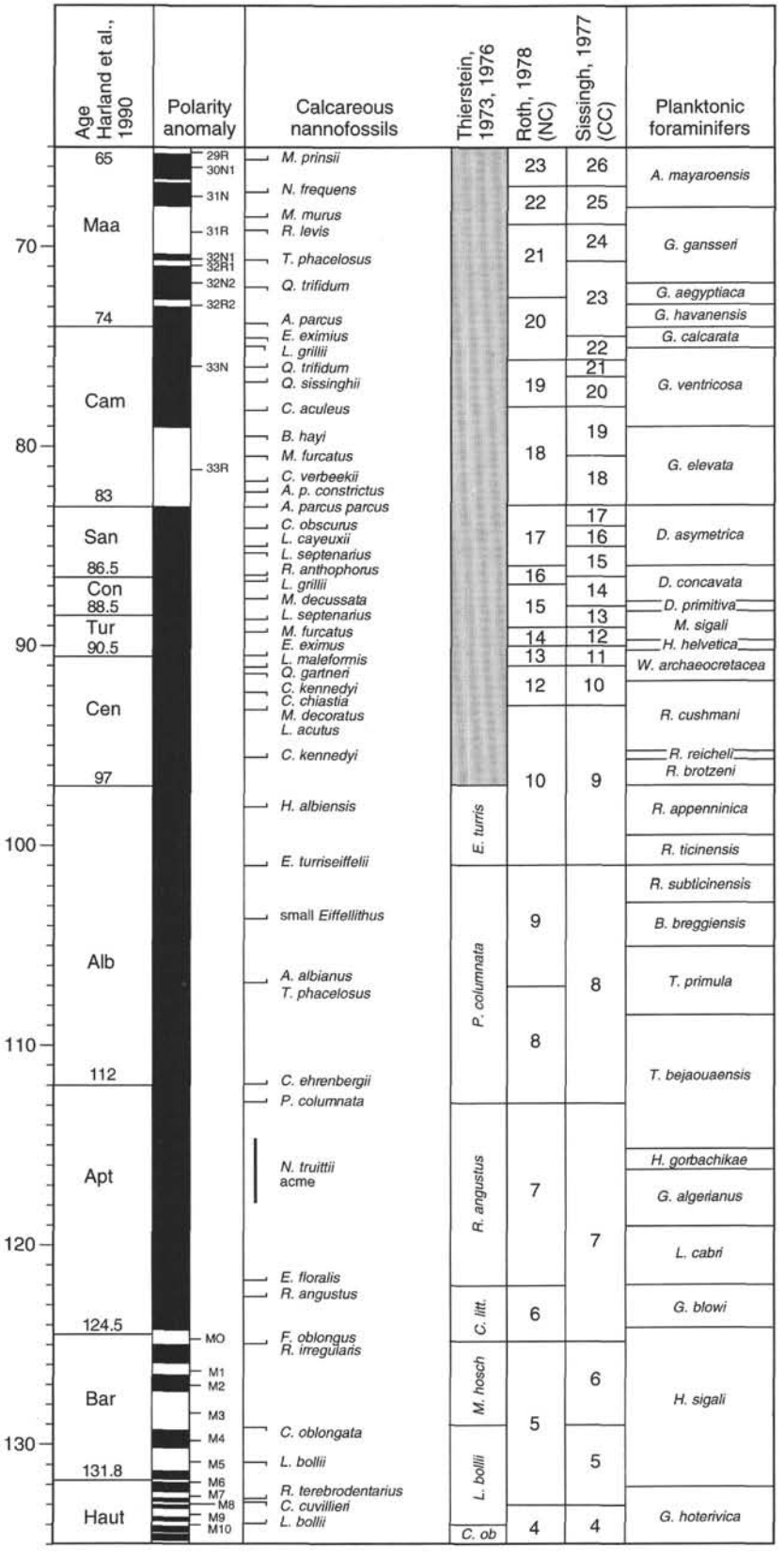

Figure 11. Correlation of Cretaceous nannofossil and planktonic foraminifer datums and zones, using the time scale of Harland et al. (1990).

PALEOMAGNETISM

Paleomagnetic studies performed on the *JOIDES Resolution* during Leg 159 included analyses of the natural remanent magnetization (NRM), isothermal remanent magnetization (IRM), and magnetic susceptibility. The bulk of the remanence and susceptibility data has been obtained from the whole-core analysis of the archive core sections and full rounds, respectively. IRM data of discrete specimens have been used in the mineralogical investigations and to supplement the whole-core remanence studies.

Laboratory Instruments

The remanence of all archive-half sections was measured using a 2G Enterprises whole-core cryogenic (WCC) magnetometer, which has an in-line three-axis demagnetization system capable of generating fields of 30 mT. The demagnetizing coils used in this system are enclosed in a mu-metal shield that attenuates the ambient field to ~100 nT. However, within the demagnetization coil, the field varied by ±100 nT due to the motion of the ship. The mu-metal shields were degaussed if the ambient field within the demagnetizing region exceeded 100 nT. Each of the sense coils in the WCC has a slightly different response curve but each effectively measures the signal over ~20 cm of core. This length corresponds to ~380 cm^3 volume of material that contributes to the remanence measured at any point in the core. Such a volume allows accurate measurement of weakly magnetized rocks and sediments, despite the background noise of the magnetometer. The WCC system is controlled by a PC-386-compatible computer running a Quick Basic program.

Discrete samples collected from the working half of the core were measured using the WCC magnetometer, in discrete sample mode, allowing measurements of up to seven samples during a single WCC run. Specimens processed on the WCC were demagnetized using a Schonstedt stationary sample alternating field (AF) demagnetizer (model GSD-1), which can generate fields up to 100 mT.

The magnetic susceptibility of whole cores was measured with a Bartington Instruments magnetic susceptibility meter (Model MS1, adapted with a MS1/CX 80-mm whole-core sensor loop set at 0.465 kHz), mounted with the gamma-ray attenuation porosity evaluator (GRAPE) and *P*-wave logger on the multisensor track (MST). The full width of the impulse response peak at half maximum is less than 5 cm.

For Leg 159 an Analytical Services Company (ASC) model IM-10 impulse magnetizer was used for IRM studies. The magnetizer was used to apply pulsed fields of between 20 and 1200 mT to discrete specimens.

Sampling Technique

Core Orientation

Core orientation of the advanced hydraulic piston cores (APC) was attempted on a case-by-case basis using a Tensor multishot tool that is mounted onto a nonmagnetic sinker bar. The Tensor tool consists of three mutually perpendicular magnetic sensors and two perpendicular gravity sensors. At the bottom of the hole, the core barrel was allowed to rest for sufficient time (2–8 min) to permit an accurate reading of the magnetic and gravity sensors. The information from both sets of sensors allows the azimuth and dip of the hole to be measured as well as the azimuth of the APC core double orientation line.

Discrete Sampling

Discrete samples in soft sediment were taken using oriented standard plastic boxes (6 cm^3). To minimize sediment deformation, the core was cut using a thin stainless spatula before pressing the plastic sampling boxes into the sediment. Cubes (10 cm^3) were cut from lithified sedimentary rocks and igneous rocks using a water-cooled saw.

Magnetic Experiments

Remanent Magnetization Measurements

Remanence measurements of sediments were performed by passing continuous archive-half core sections through the WCC. The ODP core orientation scheme arbitrarily designates the positive X-axis direction as the horizontal (in situ) line radiating from the center of the core through the space between a double line scribed lengthwise on the working half of each core liner, the positive Z-axis is down, and the positive Y-axis is 90° clockwise from the positive X-axis, looking down.

Where the rocks were weakly magnetized (<1 mA/m) and where drilling disturbance was pronounced, no demagnetization was applied to the archive-half sections, and NRM only was measured. Otherwise, two or three AF demagnetization levels (up to 30 mT) were performed on each archive-half section to isolate characteristic magnetizations. A subset of the shipboard samples was AF demagnetized in the GSD-1 to evaluate the effectiveness of the pass-through demagnetization routine in isolating a characteristic magnetization.

Magnetic Direction Determination

Both Zijderveld (1967) plots and equal-area stereographic projections were used to determine the stability of remanence of levels within the archive cores and for the discrete specimens.

Systematically steep downhole inclinations have been observed frequently in ODP cores, and are interpreted as a drilling-induced magnetization. Abrupt discordances in declinations may represent either a drilling induced effect (for instance, Leg 154 reported a radially symmetric horizontal magnetization; Curry, Shackleton, Richter, et al., 1995) or the failure of the orientation technique.

Magnetostratigraphy

The Neogene and Oligocene sediments encountered during this leg were deposited close to the Equator, so the magnetic polarity of these rocks cannot be assigned simply on the basis of paleo-inclination (Westphal et al., 1986). Thus, we have assigned polarities with confidence only where the core has been oriented by the methods described above. Magnetozones were defined on the basis of at least two successive similar polarity measurements, and the boundary between two successive magnetozones was defined by the depth at which the interpolated declination record crossed 270° or 090° declination. The ultimate time resolution of the paleomagnetic record depends on sediment accumulation rates and the resolution of the pass-through measurements, which are limited to approximately 10 cm by the coil geometry. For shipboard measurements, the measurement interval was generally 10 cm, but sometimes reduced to 5 cm when the reversal rate increased or when short events were suspected.

Where AF demagnetization isolated a consistent record of geomagnetic polarity, we offer in the site chapters an interpretation of the magnetic polarity stratigraphy of the recovered core. Magnetochron assignments were established using nannofossil and planktonic foraminiferal data using the magneto-biostratigraphic scale of Berggren et al. (in press). The geomagnetic polarity time scale of Cande and Kent (1992) provides the chronostratigraphic frame for the Cenozoic and late Mesozoic (see "Biostratigraphy" section, this chapter). For the upper part of the time scale (roughly Pliocene–Pleistocene), we use the traditional proper or place names to refer to various chrons and subchrons. For older sediments we have adopted the chronozone-labeling notation proposed by Cande and Kent (1992). The reversal boundaries are specified by the chron/subchron designation followed

by the letter "s" (for start) or "e" (for end). The combined magneto-, chrono-, and biostratigraphy that we have used is shown in Figure 10.

Magnetic Reference Directions

For tectonic studies, we are interested in the local vertical axis rotation relative to Africa. Local tectonic rotations about vertical axes have been calculated by deriving the expected declinations for the drill sites from published African paleopoles (from Westphal et al., 1986; Table 1). This direction is compared with measured declinations from oriented core sections after a simple, strike-parallel bedding correction has been applied.

Magnetic Susceptibility

Whole-core susceptibility measurements are relatively rapid to make, are nondestructive, and provide an indication of the amount of magnetizable (ferrimagnetic and paramagnetic) material in the sediment. Whole-core volume magnetic susceptibility was measured on the automated MST. Measurements were performed at the low sensitivity range (1.0) and in the SI mode, usually every 5 cm. The susceptibility response is a function of the mineralogy as well as the shape and volume of the magnetic particles within the rocks. Because magnetic susceptibility is slightly temperature-dependent, the cores were allowed to equilibrate thermally prior to analysis. The general trend of the susceptibility data curve was used to characterize the magnetic material contained within the cored sediments as well as subtle environmental and geological changes within the sediments.

Additional Magnetic Measurements

A few discrete samples were selected for IRM analysis. These experiments allowed a preliminary estimate of the magnetic mineralogy of sediments. Discrete samples were subjected to a stepwise IRM along the X axis to peak fields of 1200 mT. The resulting IRM also was measured between steps using the WCC.

STRUCTURAL GEOLOGY

Introduction

The intention of structural core descriptions made aboard ship is to systematically and quantitatively identify and describe structural information (including bedding) present in the core. Apart from the whole-round samples taken immediately after core recovery, all material, from both working and archive halves, is examined. Responsibilities of shipboard structural geologists include:

Table 1. African paleopoles and expected field directions at 3°N, 3°W, from Westphal et al. (1986).

	Pole		Site	
	°N	°E	Inc.	Dec.
Quaternary	86	150	–1	2
Pliocene	86	160	–2	1
Miocene	83	163	–8	2
Oligocene	84	170	–6	1
Paleocene–Eocene	76	199	–19	355
U. Cretaceous–Paleocene	74	209	–20	351
U. Cretaceous	69	230	–19	343
M. Cretaceous	60	248	–13	332
L. Cretaceous	56	248	–16	328
U. Jurassic–L. Cretaceous	56	246	–17	328
U. Jurassic	56	242	–21	328
M. Jurassic	60	252	–10	331
L. Jurassic	67	252	–6	338
M.–U. Triassic	64	238	–19	337
L. Triassic	53	234	–31	328
U. Permian	45	232	–38	321

1. Documentation of all structures in the core and recording of evidence for the relative timing of the various structures and diagenetic events.
2. Recording the orientation of all structures on the core face and wherever possible orienting these in three dimensions in the core reference frame.
3. Reorienting structural features from the core reference frame into a geographic framework by applying Eastman-Whipstock or Tensor multishot tool data, Formation MicroScanner (FMS) data, and primary remanent magnetization orientations.
4. Obtaining evidence from the style, geometry, and microstructure of individual structures that may bear upon the processes and conditions of deformation and finite strain.
5. Construction of plausible models of the tectonic environment and deformation history within the limitations of the shipboard data set.

Limitations

Several problems are inherent in any study of this nature. From the point of view of the identification of structures, commonly only part of the sampled interval in any one core is actually recovered. This leads to a sampling bias that for structural purposes is particularly acute; material from fault zones is often not recovered. When faulted rock from such zones is recovered, it is typically highly disturbed relative to its original position. In addition, it is often difficult to distinguish between drilling-induced disturbance and real tectonic features. In general, planar structures that traverse a core and are associated with preserved fault rock may be regarded as original tectonic features rather than drilling induced. In the case of structures in soft sediments, discretion has to be used in judging whether the structure may have been drilling induced or not. The degree of disruption of the bedding and any sedimentary structures can be used as a guide as to how disrupted the core is. In addition, the orientation of the structures relative to the side of the core liner must be considered. Cemented and/or mineral-lined fractures are likewise geological phenomena. Gently plunging striations or polishing marks may be drilling induced, but these usually can be distinguished from preexisting slickensides. Features should be considered to be drilling induced if their origin is in doubt.

Recording the orientations of the observed structures is difficult. Features must initially be oriented relative to local reference coordinates (i.e., the core liner reference frame) and subsequently corrected to geographic north and vertical. Potentially, this can be done with the multishot orientation tool (with the APC system only), paleomagnetic data, and FMS. With the APC, recovery is generally relatively complete and coring does not rotate the core within its liner to a significant degree. In the case of low recovery, correlation between core and log data can prove more difficult and may affect the ability to reorient core to geographic coordinates. An uncertainty in the position of the cored material below seafloor up to the length of the cored interval (typically 9.5 m) is possible in such cases.

Sections from individual APC core barrels should be internally consistent in relation to their local reference frames and true north. Any correction needed can be made if the multishot tool is used. For XCB and RCB coring, however, drilling disturbance and rotation within the core barrel is much more common and the multishot orientation tool cannot be used. Rotary drilling causes the rotation of individual pieces of core, such that relative rotation in any individual sections or core barrels occurs, and reorientation to geographic north may be different for each piece of core.

Core Descriptions

The shipboard structural geologist initially makes a sketch of the core on the structural core description form (Fig. 3). If any particular

feature, such as a bedding plane, a fold, a fault, etc., is measured, it is assigned a sequential reference number. If a core length is relatively devoid of features, then the structural geologist may opt not to draw this interval, but merely mark features on the structural data sheet. When a drawing is made, the reference number allows the feature to be linked to the relevant structural measurement in the data spreadsheets. Here, the location of the feature in terms of ODP curation depths is made, and the feature is identified using the codes in the accompanying structural terms table (Table 2). The core drawings have been scanned and can be found on the CD-ROM (back pocket), along with all the structural spreadsheets. Selected photographs of core faces also are found on the CD-ROM. In an attempt to achieve consistency of nomenclature, a working terminology for macroscopic features has been developed that subdivides them for the purposes of initial core description (Table 2). By subdividing core features thus, it is not implied that these features fall into distinct pigeonholes. Clearly there is gradation and even overlap, but particular aspects may be emphasized by adding modifiers, descriptive comments, and sketches. The reference or feature number for structural features written on the core description form should include the abbreviation for the structural feature in question. For example, in any given section the first fault recorded might be numbered F1, F being the code for faults taken from Table 2. This method will facilitate sorting of the data by feature within any future database system.

Fractures and faults are distinguished from each other on the basis of reasonable evidence for displacement in the latter. Reasonable evidence for displacement includes truncation or offset of passive markers and observation of slickensides and striations, fault gouge, or breccia. Veins are characterized by their fill, width, and presence or absence of an alteration halo.

Once the structure has been identified, its orientation is noted relative to the core coordinates (Figs. 12 and 13). If it is possible to reorient the core later using paleomagnetic, FMS, or mechanical methods, then these methods are noted on the table. Using these data it is possible to recalculate the geographic orientation of any structural feature. Additional comments can be added to the structural data sheet as appropriate.

Measurement of Structures

Orientations of structures are measured using a device shown in Figure 12A. It consists of a protractor-like graduated scale with a pivoted, transparent measuring arm. During measurement, one half of the arm is aligned closely against the structure of interest and the other half points to the value of the dip angle on the graduated scale.

Figure 12B shows the device being used to measure the apparent dip angle of a structure on a split core face. Dip angles refer, by definition, to inclinations from the horizontal; however, there is not a horizontal but a vertical orientation on a core. The baseline of the clinometer is therefore aligned vertically (a procedure that requires some judgment if the core material has moved within the liner or has fragmented). With the device in this alignment, the arrangement of the graduated scale is such that when the measuring arm is rotated from horizontal to vertical the readings increase from 0° to 90°. Note that this is the opposite arrangement from that found on a conventional protractor. The device reads the dip angles directly, eliminating the arithmetic necessary if it is constructed from an ordinary protractor.

The advantages of the tool apply equally to measuring a dip angle at right angles to the core face (Fig. 12C) or on some surface along which the core has broken. Such additional apparent dip readings are commonly needed to establish the true-dip value of a structure. Note that in the device illustrated here the half of the measuring arm that is aligned with the structures has been made relatively short, about 3 cm, so that it can be held against fracture surfaces without having to remove the material from the core liner. A further application of the tool is the measuring of azimuths. Figure 12D shows the base line of the device aligned parallel with the split core face, and the arm being used to measure an azimuth.

The plane normal to the axis of the borehole is referred to as the apparent horizontal plane. On this plane a 360° net is used with a "pseudo-north" (000°) at the bottom line of the working half of the core, the same convention as that used for the shipboard paleomagnetic studies. Therefore, the face of the split core lies in a plane striking 090°–270°, and dips vertically. Figure 13 summarizes the conventions used to measure azimuths and dips of structural features.

Sedimentary Bedding

Direct dip and dip direction measurements are preferred wherever possible, as they are much more precise than using apparent dips; the derivation of a plane by the combination of two apparent dips is subject to great uncertainty if the dip of the plane is shallow (Fig. 14).

Unlithified and partly lithified sediments cannot be removed easily from the core liners, so the determination and measurement of the

Table 2. Structural features identified in core and their abbreviations for use on the structural data form.

Structural feature	Abbreviation	Planar or linear orientation measured
Drilling induced	DI	
Joints	J	Joint surface
Mineral veins	V	Vein margin
Magmatic vein	MV	Vein margin
Clastic veins	CV	Vein margin
Dikes	D	Dike margin
Faults	F (N), (R)	Fault plane, normal, reverse
Slickensides	SL	Slickenside plunge and plunge direction
Breccias	B	Zone margin
Anastomosing foliation	AF	Foliation plane
Disjunctive cleavage	DC	Cleavage plane
Crenulation cleavage	CC	Cleavage plane
Folds	Fo	Fold plane and hinge line
Slump fold	SFo	Fold plane and hinge line
Brittle shear zone	BSZ	Shear zone margin
Ductile shear zone	DSZ	Shear zone margin
Crystal plastic fabric	PF	Shear zone margin/foliation plane
Crystal mineral lineations	ML	Lineation plunge and plunge direction
Magmatic fabrics	M	Foliation plane and mineral lineation
Mineral shape fabric	MF	Foliation plane and mineral lineation
Compositional and/or textural variation	CTV	Surface between zones of differing color and texture
Gradational boundary	GB	Approximate planar boundary orientation
Compositional layering	CL	Interlayer surfaces
Igneous contacts	IC	Contact surface
Sedimentary bedding	SB	Bedding planes
Water escape structure	WES	NA
Stylolites	ST	Stylolite planes

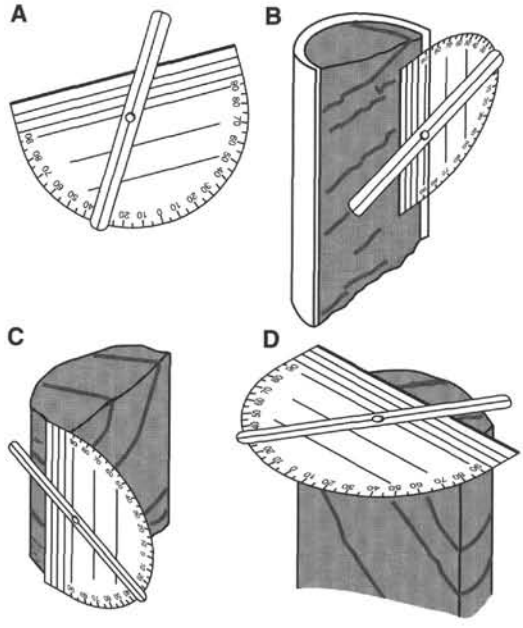

Figure 12. **A.** Drawing of a device for measurement of core-structure orientations. **B.** Device being used to measure the dip of a structure on the face of a split core. **C.** Device being used to assess the dip of a structure as seen at right angles to the split-core face. **D.** Measuring the azimuth of a structure as seen on an upper surface of a core.

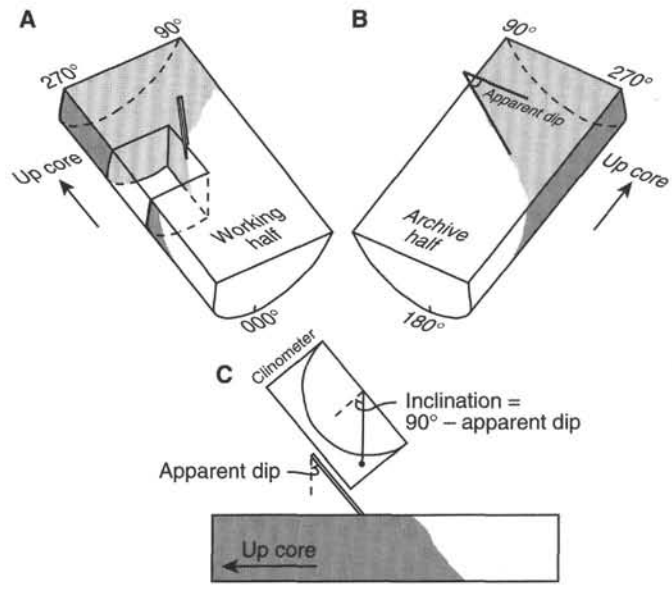

Figure 13. Diagram showing the conventions used in measuring azimuths and dips of structural features in cores and the techniques adopted for measuring structural planes in three dimensions in the core reference frame. The core reference frame conventions for the working half and the archive half of the core are shown in (**A**) and (**B**), respectively. The E–W (core reference frame) apparent dip of the feature was measured first, generally on the face of the archive half (sometimes on the working half). The data were recorded as an apparent dip toward either 90° or 270°. A second apparent dip is measured by making a cut parallel to the core axis but perpendicular to the core face in the working half of the core (A). Note that cuts are normally much smaller than that shown in the diagram. The feature is identified on the new surface and the apparent dip in the N–S direction (core reference frame) marked with a toothpick. The apparent dip is measured with the modified protractor (**C**) and quoted as a value toward either 000° or 180°. True dip and dip direction of the surface in the core reference frame are calculated from the two apparent measurements.

orientation of bedding planes and so forth cannot be made directly without disturbance of the core. The apparent dip in the plane of the cut surface is measured using a protractor or a clinometer (Fig. 12) and its sense recorded (i.e., whether the bedding plane dips to the left or to the right when looking up the axis of the core). A vertical incision is then made, using a metal scoop, parallel to the axis of the core, and a quarter-round sample (including the bedding plane) is temporarily removed to expose a new face perpendicular to the original split-core surface. A second apparent dip is then measured on this new face, and the sense (i.e., whether the apparent bedding surface dips toward the "top" or "bottom" of the core) recorded. The potential errors inherent in this technique (assuming that the apparent dips can be measured to the nearest degree) are high for gently dipping planes, but are much lower for moderately dipping features (Fig. 14).

"True" dips and dip directions (relative to core coordinates) can be derived from the apparent measurements using stereographic projections, calculations, or diagrams. The normal to a plane defined by two lines can be calculated simply from the cross product of the two lines. The orientation of this plane gives the dip direction and dip of the observed structure. Alternatively, assignment may be made later, at the same time that correction is made to geographic coordinates, when paleomagnetic and/or downhole geophysical logging information becomes available.

Veins, Fractures, and Other Features

The orientation of all planar features in the core is determined in the same way as for bedding, assuming that the core is essentially vertical. If a correction is to be made, the amount and direction of hole deviation must be obtained from the downhole inclination tools (Tensor tool), and both the strike and dips of the core adjusted accordingly. For the majority of ODP holes the inclination is close to vertical (<5°), and this rather complicated procedure can be ignored without the introduction of serious errors.

Linear structures such as striations can be measured either directly by their azimuth and angle of plunge, or indirectly by means of their pitch on a previously measured plane. The sense of movement of some linear structures can be ascertained, allowing the distinction between components of normal vs. reverse and/or sinistral vs. dextral motion. The magnitude of displacement may be visible, and can be measured directly, if the fault surface is visible, or calculated from the apparent offset on the cut surface of the core.

Mineral foliations are measured in the same way (Fig. 15). Linear structures such as slickensides are measured either directly by their azimuth and amount of plunge, or indirectly by means of their pitch on a previously measured plane. The pitch of a line is generally measured from the strike of a plane, in this case such that the dip direction is 90° clockwise from the strike. Reference also can be made to various physical and magnetic properties of the core (specifically, anisotropies of seismic velocity and magnetic susceptibility, respectively) to help characterize and constrain rock fabrics in the post-cruise period.

Depths are recorded at the middle of a feature, which will typically be the depth of the feature's intersection with the center line of the core, if the feature cuts fully through a core. Where several features of the same type occur at the same depth or in the same core piece, confusion is avoided by the use of the numbering system linked to the

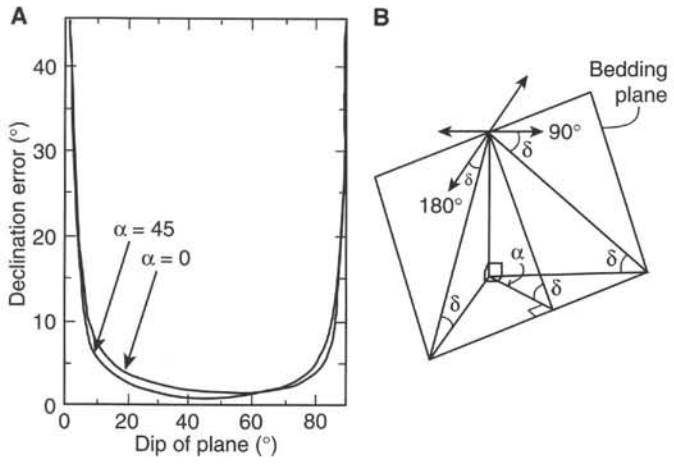

Figure 14. **A.** Estimation of uncertainties involved in strike measurements derived from the combination of two apparent dips. **B.** Representation of a planar structural feature relative to the core liner reference frame. The crossed direction arrows represent the plane perpendicular to the length of the core. δ is the apparent dip along perpendicular planes cut in the core.

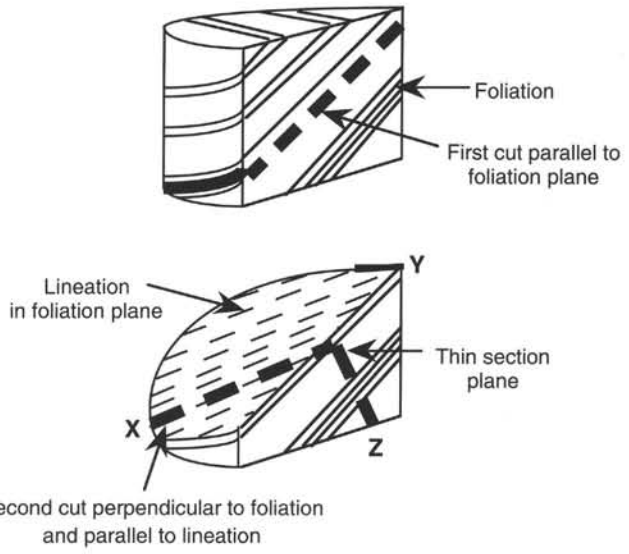

Figure 15. Orientation of cuts necessary to obtain correctly oriented thin sections for structural purposes.

structural feature abbreviations (e.g., V1, V2, etc., in the case of veins). These numbers have no chronological significance.

Thin-section Descriptions

Thin sections are examined (1) to confirm macroscopic descriptions of ductile and brittle structures; (2) to provide kinematic information; (3) to determine time relationships between deformation and dynamic metamorphism; and (4) to provide coverage of major structural zones and a representative section of downhole variations.

Where possible, sections are oriented with respect to the core (i.e., the original attitude of the vertical is preserved), and samples are cut perpendicular to the foliation and parallel to any extensional lineation, as this is the plane that best displays both shear-sense indicators and the preferred dimensional orientation of minerals (Fig. 15). This information is entered on the standardized structural data sheet.

Methods of Core Orientation

One of the principal limitations of core-based structural studies is that the core pieces are not oriented with respect to azimuth. In the absence of azimuthal data, it is not possible to assess directly the significance of, for example, microstructures, petrofabrics, or fault kinematic data from the core in the context of larger scale tectonic features inferred by other geological or geophysical means. Many other core-based studies (e.g., paleomagnetic data) are similarly hampered. Thus, a variety of techniques is used to reorient core material into true geographic coordinates.

1. Formation MicroScanner (FMS)

The FMS logging provides an "image" of the borehole wall by measuring the variations in resistivity using pads pressed against the wall. It carries a magnetometer that allows orientation of the processed images. The FMS is able to distinguish sedimentary bedding and can be used as a structural tool (e.g., MacLeod et al., 1992, 1994). The difference between the diameter of the borehole and that of the core is such that the correlation of individual features between them may be difficult; they can be used most successfully for orientation purposes when, for example, regularly inclined bedding or a single, regular joint pattern can be recognized on downhole images and correlated with the core-derived data.

The FMS downhole logging tool, described in the "Downhole Measurements" section (this chapter), generates high-resolution electrical images of the borehole wall. These images are oriented with respect to geographical coordinates, because the tools carry triaxial magnetometers. Comparison of the features in the cores and on the logs allows the former to be reoriented from the core reference frame to geographical coordinates. Paleomagnetic data can be reoriented in the same way and provide a means of detecting tectonic rotations, which otherwise have to be assumed to be zero. The methodology of core reorientation using downhole logs is described in detail in MacLeod et al. (1992, 1994), and applied for structural data from Leg 135 by MacLeod (1994) and for paleomagnetic data by MacLeod et al. (1992, 1994). Its principal disadvantages are its inapplicability if there are no distinctive markers in the borehole, and that detailed comparison with the logs can only be made post-cruise. Shipboard scientists are therefore restricted to attempting reorientation of core pieces relative to the primary magnetization vector of core samples and to results obtained from the Tensor tool.

2. Paleomagnetic Data

Previous workers often have attempted to use the primary magnetization vector of young core samples to reorient core, assuming that this vector is coincident with the present-day Earth's field; however, this neglects the possible effects of secular variation and assumes that no tectonic rotation of the sample, be it on a local or regional scale, has occurred. Paleomagnetic analysis provides a way of orienting individual sections of core on a small scale and is especially useful for basement cores obtained by XCB or RCB coring, which typically recovers contiguous pieces of core ranging from only a few centimeters up to about 1 m in length. Data from the routine analysis of the archive halves of the core made by the shipboard paleomagnetists using a cryogenic magnetometer with demagnetization up to 25 mT can be used to orient sections of core. The declination and inclination of the natural remanent magnetization determined by these methods can be used to orient larger pieces of core. In some cases where the magnetization has been acquired prior to tectonic rotation, the whole core will show a consistent magnetic azimuth, but this will be different from the present-day field direction. These techniques do not correct for secular variations in the Earth's magnetic field. For samples that acquired their magnetic characteristics rapidly (i.e., igneous rocks), variation in the order of +15° in declination and inclination from the

present-day field is to be expected. Nevertheless, in this case the magnetic properties within the single rapidly emplaced lava flow should be constant. Table 3 summarizes the steps in the paleomagnetic reorientation procedure.

3. Multishot and Tensor Orientation Tools

The principal tool used to chart the deviation of the hole is the Tensor tool. This provides frequent measurements of the direction and degree of deviation of the hole from the vertical. The degree of inclination of the hole is measured using two accelerometers. The vertical acceleration is compared with the acceleration caused by gravity to calculate inclination. Measurement and data retrieval are done electronically at pre-determined time intervals. Accurate measurements currently assume no vertical acceleration by the tool in the hole. The multishot orientation tool provides the principal backup system to the Tensor tool and consists of a compass that is lowered downhole and photographed next to the plastic core liner, such that the orientation of the reference marks on the liner relative to magnetic north are visible. The vertical deviation of the hole is measured by a pendulum. For structural studies, the multishot tool can be used only with the APC system, and therefore only in the uppermost (<200–250 mbsf), barely lithified, sedimentary sections of a hole, where it provides important information on the azimuth of the recovered core.

ORGANIC GEOCHEMISTRY

The shipboard organic geochemical investigations for Leg 159 include (1) real-time monitoring of the volatile hydrocarbons as required by ODP safety considerations, (2) measurement of the inorganic carbon concentration to determine the amount of carbonate in the sediments, (3) elemental analysis of nitrogen and total carbon, and (4) determination of free hydrocarbons, pyrolyzable hydrocarbons, and maturity of organic matter. A more detailed description of the analytical procedures is given in Emeis and Kvenvolden (1986) and in the "Explanatory Notes" chapter of Leg 146 (Westbrook, Carson, Musgrave, et al., 1994).

Hydrocarbon Gases

As required by safety and pollution prevention considerations, the concentrations of the low molecular weight hydrocarbons methane (C_1), ethane (C_2), and propane (C_3) were monitored in the sediment cores at intervals of approximately 10 m. A 5-cm^3 sample was removed from the end of the core immediately after it arrived on deck. The sample was placed in a glass vial that was sealed and then heated to 70°C for at least 30 min (Kvenvolden and McDonald, 1986).

The gas samples were injected into a Hach-Carle AGC series 100, Model 211, gas chromatograph equipped with a flame ionization detector and a 6 ft × 1/8 in. steel column packed with Porapak N:Q (80%/20%). The gas chromatograph has a detection limit for methane of 0.1 ppm. Details of this method and the complete configuration of the instrument are given in the "Explanatory Notes" chapter of Leg 112 (Suess, von Huene, et al., 1988). When higher concentrations of gas were found, we used the Hewlett-Packard 5890A Natural Gas Analyzer (NGA), equipped with a 6 ft. × 1/8 in. steel column packed with Poropak T, a 3 ft × 1/8 in. stainless steel column with a 13× molecular sieve, a 6 ft × 1/8 in. steel column packed with 80/100 mesh Hayesep R (acid wash), and a DB "series" (1-mm film thickness, J&W). Automatic valve switching was controlled by a Hewlett-Packard 3392 Integrator, which also recorded and integrated count rate, and provided a rapid determination of oxygen, nitrogen, carbon dioxide, and hydrocarbons from methane (C_1) to hexanes (C_6).

Inorganic Carbon

Inorganic carbon was determined using a Coulometrics 5011 Carbon Dioxide Coulometer equipped with a System 140 carbonate carbon analyzer. Approximately 70 mg of freeze-dried, ground sediment of known weight was reacted in a 2N HCl solution. The liberated CO_2 was titrated in a monoethanolamine solution with a color indicator, while the change in light transmittance was monitored with a photodetection cell.

The percentage of calcium carbonate was calculated from the inorganic carbon content assuming that all the CO_2 evolved was derived from dissolution of calcium carbonate by the following equation:

$$CaCO_3 = IC \text{ (inorganic carbon)} \cdot 8.33 \quad (1)$$

No corrections were made for other carbonate minerals such as siderite or dolomite.

Elemental Analysis

The nitrogen and total carbon (TC) content of the sediment samples was determined by a Carlo Erba Model NA 1500 Nitrogen-Carbon-Sulfur (NCS) Analyzer. Both nitrogen and total carbon data were corrected to an internal standard (Estuarine Sediment, standard reference material no. 1646; National Institute of Standards and Technology, U.S.A.). In the NCS Analyzer, freeze-dried and ground samples were combusted at 1000°C in an oxygen stream. Nitrogen oxides were reduced to N_2, and the mixture of CO_2, SO_2, and N_2 was separated by gas chromatography and quantified with a thermal conductivity detector. Total organic carbon (TOC) was calculated by the

Table 3. A summary of the steps in converting measurements of structures observed in split cores to real geographic coordinates.

1. Identify features and measure apparent dips on archive-half of core.
2. Look for auxiliary surfaces that provide further orientation information.
3. If necessary, refer to working-half of core for auxiliary information.
4. Derive true dip and azimuth orientations (e.g., using Stereonet Plotting Program of R.W. Allmendinger, plot apparent dip directions and angles as lines, and find cylindrical best fit).
5. Correct dip angles for deviation of drill hole from vertical, if this information is available from downhole tools. Amount and direction of dip will affect both the dip and strike information measured from the core.
6. Select representative piece from continuously oriented part of core and pass through the cryogenic magnetometer. If the core section underwent little differential rotation during drilling, it may be reasonable to average the entire section. Derive the magnetic declination.
7. If the paleomagnetic declination falls between 000° and 180°, subtract its value from the working azimuths to obtain the real strike, adjusting the dip direction as appropriate. If the adjusted paleomagnetic declination falls between 180° and 359°, add its value to the working azimuths, and adjust dip directions. These operations are conveniently performed stereographically (by rotating the orientations of the planes around a vertical axis by the required amount and in the appropriate direction), which allows both visual checking of the manipulation and direct printing of the results.
8. Record paleomagnetically corrected real strike and true dip.

difference between total carbon (TC) from the NCS and inorganic carbon (IC) from the coulometer:

$$TOC = TC - IC \quad (2)$$

Organic Matter Characterization and Maturity Determination

Organic matter type, thermal maturity, and hydrocarbon-producing potential were assessed using a Delsi Rock-Eval II plus TOC instrument (Espitalié et al., 1986). The Rock-Eval II uses a temperature-programmed whole-rock pyrolysis technique to determine the amount (in mg per gram rock) of free hydrocarbons (S_1, detected at 300°C for 3 min), of pyrolyzable hydrocarbons from kerogen (S_2, from 300° to 600°C with continuous temperature increase of 25°/min), and the quantity of CO_2 (S_3, from 300° to 390°C) released from about 100 mg of ground and weighed sediment. Hydrogen indices [HI = (100 × S_2)/TOC] and oxygen indices [OI = (100 × S_3)/TOC] were calculated using TOC values obtained by elemental analyses, and S_2 and S_3 yields from Rock-Eval pyrolysis after correction to an internal standard (55000, IFP). A maximum temperature (T_{max}) value is obtained during pyrolysis at which kerogen yields the maximum amount of hydrocarbons during the evolution of S_2. T_{max} values were used as a measure of the thermal maturity of sedimentary organic matter after correction to an internal standard (55000, IFP).

INORGANIC GEOCHEMISTRY

Interstitial Water Sampling and Analyses

Shipboard interstitial water analyses were performed on 5- to 15-cm-long whole-round sections that were cut soon after the core arrived on deck. Interstitial waters were collected using a titanium and stainless steel squeezer (Manheim and Sayles, 1974). Prior to squeezing, the surface of each sample was carefully scraped with a spatula to remove potentially contaminated exteriors. The sample was then placed into a titanium cylinder on top of a Whatman No. 1 filter that had been rinsed in deionized water to remove processing acids. A second, similarly treated filter paper and a stainless steel piston were placed on top of the sample in the cylinder. Pressure, up to 40,000 lb per square in., was applied with a hydraulic press to force the interstitial water out of the sediment. The pore water, collected in a plastic syringe attached to the bottom of the assembly, was passed through an in-line 0.45-mm Gelman polysulfone disposable filter. Samples that could not be analyzed immediately were stored in polystyrene vials and refrigerated pending analysis. Aliquots for future shore-based analyses were heat-sealed in acid-washed plastic tubes and glass ampoules.

Routine analyses of interstitial water samples were performed as follows: Potentiometric alkalinity titration and pH measurements were conducted using a Metrohm autotitrator and a Brinkman combination pH electrode immediately after the sample was retrieved. Chloride, calcium, and magnesium concentrations also were determined by titration. International Association of Physical Sciences Organizations (IAPSO) standard seawater was used for calibration. Reproducibility for these analyses is expressed as 1 σ of the means for multiple determinations of IAPSO standard seawater. These values are <1.5% for alkalinity and chloride, <2% for calcium and magnesium. A more detailed description of the procedures is given by Gieskes et al. (1991). Ammonium concentrations and dissolved silica concentrations were determined using colorimetric methods described by Gieskes et al. (1991).

During Leg 159, sulfate analyses were performed by ion chromatography. Potassium, calcium, and magnesium were also analyzed by ion chromatography. IAPSO standard seawater was analyzed to monitor data quality during each ion chromatograph run. Over the course of Leg 159 the average measured IAPSO values were: potassium, 10.66 ± 0.13 mM; magnesium, 55.95 ± 1.7 mM; calcium, 10.96 ± 0.37 mM; and sulfate, 29.2 ± 1.0. Stated uncertainties are ±1 standard deviation of the replicate analyses. An inter-comparison of calcium and magnesium concentrations determined by both ion chromatography and titration during Leg 159 is shown in Figures 16 and 17, respectively. The paired calcium and magnesium data both plot close to the 1:1 line, demonstrating that both methods can yield reliable calcium and magnesium data. However, there is a better agreement in the magnesium than in the calcium data. This possibly is because the highest concentration standards prepared from IAPSO seawater did

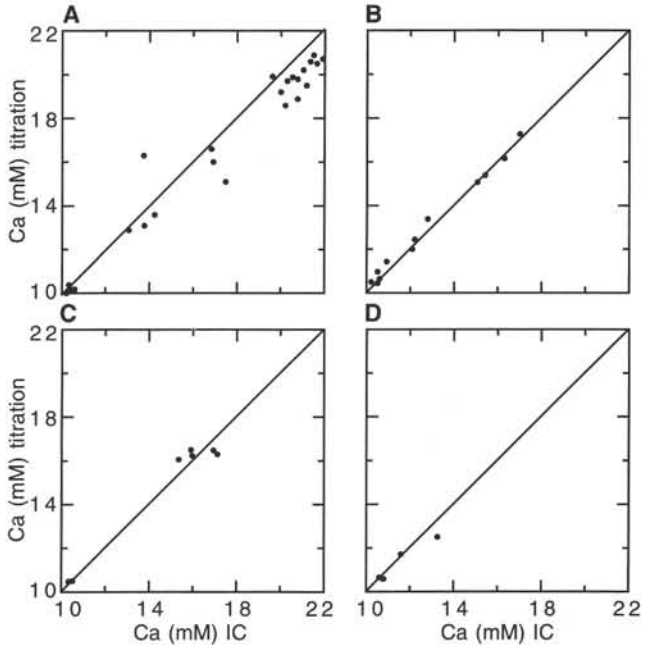

Figure 16. Comparison of calcium interstitial water concentrations determined by ion chromatography (IC) and titration from Leg 159. **A.** Site 959. **B.** Site 960. **C.** Site 961. **D.** Site 962.

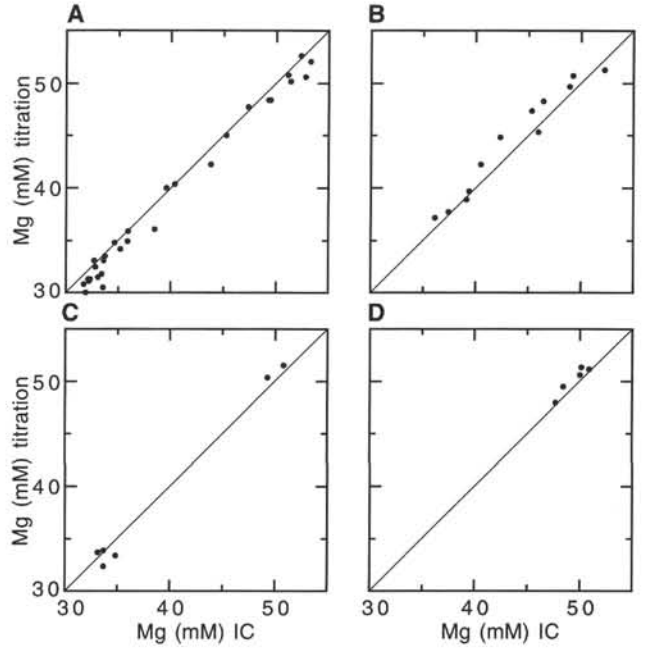

Figure 17. Comparison of magnesium interstitial water concentrations determined by ion chromatography (IC) and titration from Leg 159. **A.** Site 959. **B.** Site 960. **C.** Site 961. **D.** Site 962.

not always span the full range of Ca concentrations of interstitial water samples. In general, calcium and magnesium concentrations, as determined by titration, are reported in the site chapters. When ion chromatograph data are reported for these elements, this is stated explicitly in the site chapter table captions.

In addition to the routine analyses, strontium, iron, and manganese concentrations of interstitial waters were measured using flame atomic absorption spectrophotometry (Varian Spectra AA-20). Strontium standard and sample concentrations were determined on aliquots diluted 1/10 with a 1000 ppm lanthanum chloride solution as an ionization suppressant. Strontium was determined by atomic absorption using a nitrous oxide-acetylene flame. Iron and manganese samples were acidified immediately after squeezing to prevent precipitation of iron oxyhydroxides. This was accomplished by the addition of 100 µL of concentrated HCl to each ~5 mL sample aliquot. Manganese concentrations were determined on aliquots diluted with 1000 ppm lanthanum chloride as an ionization suppressant. Samples and standards for iron and manganese were diluted as necessary to keep within the linear working range of the instrument. Iron and manganese were determined by atomic absorption using an air-acetylene flame. Standard solutions for all flame AA techniques were made in a seawater matrix to match matrix composition to the samples. The reproducibilities of these techniques (as determined by replicate analyses of IAPSO seawater or another suitable standard) are <4% for strontium, 2%–3% for iron, and 2%–3% for manganese. Chemical data for interstitial waters are reported in molar units.

PHYSICAL PROPERTIES

Introduction

General Objectives

The principal objectives for the physical properties measurements can be grouped as follows:

1. To provide high-resolution data for construction of a complete stratigraphic section and an integrated view of the lithology;
2. To determine stress and deformation history of lithologic units for control on the mass accumulation rates, definition of erosional unconformities, and delineation of overconsolidated units as compared with diagenetically altered units;
3. To cross-correlate and calibrate shipboard analyses. Analyses of all physical properties were made on common sample intervals to avoid aliasing of data sets;
4. To calibrate downhole logs. Bulk density, porosity, acoustic velocity, and natural gamma radiation (NGR) data from core samples are all valuable for core-log data integration.

Laboratory Measurements

Multisensor Track

Continuous measurements made with the multisensor track (MST) provide an important link between downhole logging and laboratory analyses. The MST incorporates the magnetic susceptibility meter, gamma-ray attenuation porosity evaluator (GRAPE), *P*-wave logger (PWL), and natural gamma radiation (NGR) tool.

Immediately after the core was cut into the 1.5-m sections, whole-round samples designated for shipboard geochemical analyses were removed, resulting in discontinuous MST data. To obtain thermal equilibrium, the core was left at room temperature for 4 hr. Individual unsplit core sections were placed horizontally on the MST, which moves the section through the four sets of sensors. Measurements with the GRAPE and PWL were made while the track was moving, and magnetic susceptibility and NGR while it was stationary. The whole system is operated from IBM or PC clones, and the data are automatically recorded on the hard disk. The software controlling the MST allows the operator to specify the position of the first measurement and the sampling interval, but not the position of the last measurement. Thus the last measurement of each section may be biased by an edge effect unless the operator entered a shorter length than the actual length of the section being measured. Descriptions of the particular sensors are presented below.

The description of the magnetic susceptibility sensor is presented in the "Paleomagnetism" section (this chapter). The results of magnetic susceptibility measurements are included in the "Paleomagnetism" chapters for the respective sites.

The GRAPE makes measurements of bulk density by comparing attenuation of gamma rays through the cores with attenuation through an aluminum standard (Boyce, 1976). The GRAPE data were most reliable in APC and undisturbed XCB and RCB cores. In XCB and RCB cores where the sediment does not fill the liner, the GRAPE measurements have no meaning in terms of density estimation. However, these measurements may be used in conjunction with discrete density measurements to provide an estimate of core diameter and hence to correct magnetic susceptibility and natural gamma measurements for the reduction in volume. The GRAPE is calibrated each 24 hr with an aluminum and air standard. GRAPE data were obtained at 2-cm intervals on all sections. The data reported here are corrected for the fact that in high porosity sediment one cannot make the assumption that the sample is close to quartz in atomic number (i.e., Boyce-corrected density). The density data are edited by removing all values less than 1.0 g/cm^3 (i.e., density of pure water). Data quality depends strongly on the core diameter: lower density values are obtained in sections where the core diameter is small and/or the core liner contains many voids. Therefore, only the maximum values of the Boyce-corrected bulk density are considered.

The PWL transmits a 500-kHz compressional-wave pulse through the core at a repetition rate of 1 kHz. The transmitting and receiving transducers are aligned perpendicular to the core axis. A pair of Linear Variable Displacement Transducers (LVDT) monitor the separation between the compressional wave transducers; variations in the outside diameter of the liner therefore do not degrade the accuracy of the velocities. Only the APC and undisturbed XCB cores were used for PWL data collection. XCB and RCB cores generally failed to completely fill the core liner, which made the PWL ineffective. The *P*-wave standard filled with distilled water was run periodically. *P*-wave velocity was measured at 2-cm intervals. No correction on the velocity is made automatically by the operating system at this stage. The velocity data are edited in two steps: first, data with a signal quality less than 40 are removed. The signal quality is a measure of how well the acoustic signal traveled through the core, and it can vary from 0 to 255. Second, velocity values less than 1.45 km/s (i.e., the velocity of seawater at 0°C) are deleted.

Natural gamma radiation (NGR) analysis is a function of the random and discrete spontaneous decay of radioactive atoms, the types and concentrations of radioactive elements present, detector type and geometry, and the time period of the analysis (Hoppie et al., 1994). NGR data are mainly used for three purposes: (1) reliable core-log correlation, (2) intersite and regional stratigraphic correlation, and (3) data for lithologic studies. The NGR tool consists of four 7.6 × 7.6 cm cylindrical NaI scintillation gamma-ray detectors, each housed with photomultiplier in copper tubing. The background radiation values for each counting channel that were subtracted from subsequent measurements were based on 50 10-s counts and are presented in Table 4. NGR was measured at 15-cm intervals in at least one hole at each site, with 10- or 30-s counting periods. Corrections for sampling volume as proposed by Hoppie et al. (1994) were not made due to time constraints; thus, the data are reported in counts per second (cps).

Thermal Conductivity

The thermal conductivity of cored material was measured using the needle probe method, in full-space configuration (whole-round core) for soft sediments (Von Herzen and Maxwell, 1959), and in

Table 4. Background radiation values for each counting channel of the NGR tool.

Counting channel (keV)	Background radiation x ± sd (cps)
200–500	5.39 ± 1.13
500–1100	2.13 ± 0.48
1100–1590	0.73 ± 0.23
1590–2000	0.21 ± 0.13
2000–3000	0.29 ± 0.15
Total	8.74 ± 1.29

Note: x ± sd = arithmetic mean value ± standard deviation.

half-space configuration (split core) for lithified sediments (Vaquier, 1985). All measurements were made after the cores had equilibrated to laboratory temperature.

Data were reported in units of $Wm^{-1}C^{-1}$, and have an estimated error of less than 15%. The data were not corrected for in situ pressure and temperature, because these corrections were considered to be significantly smaller than errors in the measurements. Errors in measurements were partially caused by technical problems with the equipment, but also by drilling disturbances, cracks and fractures in sediments, and water in the liner.

Data were acquired using a Thermcon-85 unit interfaced to an IBM-type PC. This system allows up to five probes to be connected and operated simultaneously. At the beginning of each test, sample temperatures were monitored until the background thermal drift was less than 0.02°C/min. Once the samples reached thermal equilibrium, the heater circuit was closed and the temperature rise in the probes was recorded. The thermal conductivity (k), calculated from the rate of temperature rise, is the coefficient that gives the rate of heat transfer (Q) across a given steady-state temperature difference (ΔT) over a given distance (Δx) in the material, in a one-dimensional sense:

$$Q = k \cdot \frac{\Delta T}{\Delta X} \tag{3}$$

Units of Q (heat flow) are $Wm^{-2} = Wm^{-1}C^{-1} \cdot °C/m$ (SI system). The measured downhole temperature gradient values obtained from the ADARA temperature tool were multiplied by the mean thermal conductivity to calculate an average heat flow. The results of heat flow measurements are included in the "Site Geophysics" sections for the respective site chapters.

"Full-space" Measurements

Needle probes containing a heater wire and a calibrated thermistor were inserted into the working half of the core through small holes drilled in the core liners before the sections were split. A minimum of two to three measurements were taken per full core. Measurements of thermal conductivity using the full-space method were performed until the sediment became too lithified to insert the needle probes. A thermally conductive compound (Thermal joint compound, Type 120) was occasionally used to improve the thermal contact between the needle and the sample in well-lithified sediments. Bright orange dots mark the location of places where thermal compound was used, on both working and archive halves. The full-space needle-probe method of measuring k employs the transient heating, which is a result of a steady line source of heat in a probe. After the heating has begun, the changing temperature $T(t)$ of the probe is related to the thermal conductivity (k) of the surrounding material by (Von Herzen and Maxwell, 1959):

$$T(t) = \left(\frac{q}{4\pi k} \cdot \ln(t) + L(t)\right) \tag{4}$$

where t = time and q = heat input per unit length of wire per unit time. Units of $T(t)$ are $°C = Wm^{-1}/Wm^{-1}C^{-1} \cdot 1 + °C$.

The function $L(t)$ describes a linear change in temperature with time. It includes the background temperature drift, any linearity that results from instrumental errors, and the geometrical inadequacies of the experiment, which include the finite length of the probe and sample. After the heater has been on for about 60 s, the needle probe response is close to that of a line source with constant heat generation per unit length. Temperatures recorded during a time interval of 60–240 s are fitted with the least-squares technique to the appropriate equation. The thermal conductivity is derived from the slope of temperature vs. the logarithm of time. If the substrate on which the sample is placed were a perfect thermal insulator, the rise in temperature with time at the needle probe would be exactly twice that experienced by the probe in an infinite medium having the same thermal conductivity of the sample.

All measurements were corrected for a linear offset between measured and true thermal conductivities, determined from a series of tests using full-space methods with three standards of known conductivities (Ratcliffe, 1959; Fig. 18). For quality control, one probe was used with a standard of known conductivity during each run. The standards used were black rubber, red rubber, and macor ceramic.

"Half-space" Measurements

Lithified samples were selected from the archive half to prevent contamination of samples used for chemical analysis by the thermally conductive compound (Thermal joint compound, Type 120), which was used to improve the thermal contact. Samples contaminated by thermal compound are labeled. Measurements were made with a needle probe placed between the flat surface of the sample and that of an epoxy block, which has a relatively low conductivity (Sass et al., 1984; Vaquier, 1985). The contact areas of the samples were finely smoothed with sandpaper. All measurements were conducted in a distilled water bath with a water temperature greater than 18°C to reduce thermal drift during the tests, to keep the samples saturated, and to improve the thermal contact between the needle and the sample.

The data collection and reduction procedures for half-space experiments were identical to those for full-space experiments. The half-space needle-probe method requires a correction factor to account for the geometry of the experiment, as the medium is assumed to be semi-infinite (Sass et al., 1984; Vaquier, 1985) rather than fully infinite. To a first approximation, results derived with a half-space apparatus may be used to determine the true thermal conductivity of the sample (k_t) if the data are assumed to follow the relationship described by Equation 5:

$$k_t = F \cdot k_a \tag{5}$$

where F = correction factor, and k_a = true thermal conductivity of the sample. Units of k_t are $Wm^{-1}C^{-1} = 1 \cdot Wm^{-1}C^{-1}$.

Through tests with standards of known conductivities, correction factors were determined and taken to be linear as a first approximation for each of the three needles in the half-space bath (Lee, 1989). All measurements were corrected for true thermal conductivities, determined from a series of tests using half-space methods with standards of known conductivities (Fig. 19). Thermal conductivity probes were calibrated by conducting measurements on three standards of known thermal conductivities. For quality control, one probe was used with a standard of known conductivity during each run. The standards used were black rubber, red rubber, and macor ceramic.

Index Properties

The relation between the weight and volume of fluid and solid components of sediments and rocks is reflected in index properties (Fig. 20). By measuring the wet and dry mass and volume of a sam-

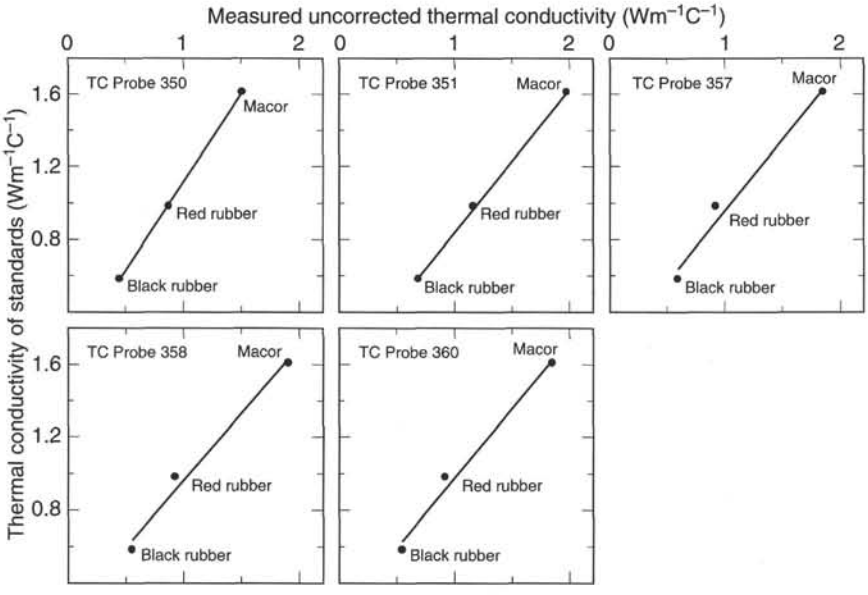

Figure 18. Thermal conductivity calibration data from full-space standards for probes 350, 351, 357, 358, and 360. The linear regression equations for the respective probes are as follows: probe 350, $y = 0.1039 + 0.97692$; probe 351, $y = 0.0019189 + 0.79501$; probe 357, $y = 0.13993 + 0.48346$; probe 358, $y = 0.19335 + 0.73574$; and probe 360, $y = 0.17416 + 0.76799$. The curve fit between equation and data is 0.99997 for probe 350, 0.99979 for probe 351, 0.99015 for probe 357, 0.99165 for probe 358, and 0.99330 for probe 360.

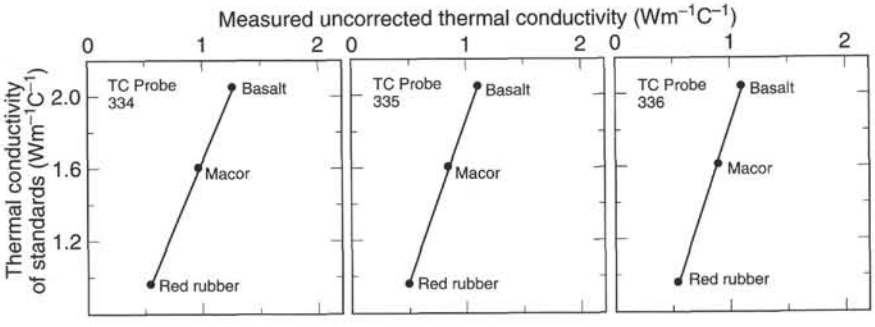

Figure 19. Thermal conductivity calibration data from half-space standards for probes 334, 335, and 336. The linear regression equations for the respective probes are as follows: probe 334, $y = 0.13267 + 1.5285$; probe 335, $y = 0.074259 + 1.8003$; and probe 336, $y = -0.069687 + 1.9222$. The curve fit between equation and data is 0.99996 for probe 334, 0.99898 for probe 335, and 0.99943 for probe 336.

ple, a number of interrelated parameters can be calculated. For Leg 159, these parameters are bulk, solids-grain and dry density, water content based on wet and dry mass, porosity, and void ratio (Table 5 and Fig. 20). Table 5 shows two columns of formulas. The first column presents formulas for nonsaline environments and should be considered when evaluating the relations between the various index properties. Pore waters of marine sediments and rocks contain dissolved salts that may change phase during drying of the sample; thus, a correction for pore-water salinity must be included. These formulas are shown in column two of Table 5. The determination of water content followed the methods of the American Society for Testing and Materials (ASTM) designation D2216 (ASTM, 1989). All measurements were corrected for salt assuming a pore-water salinity of 35‰.

Sample mass was determined aboard ship to a precision of ±0.01 g using the Scitech electronic balance. The sample mass was counterbalanced by a known mass such that only mass differences of less than 5 g usually were measured. Volumes were determined in three ways: from the Quantachrome Penta-Pycnometer, by sampling a constant volume, or by measuring the dimensions of cubic samples. The Quantachrome Penta-Pycnometer (helium displacement pycnometer), which measures volumes to an approximate precision of ±0.02 cm^3, was most often used. Sample volume measurements were repeated until two consecutive runs yielded volume differences of less than 0.02 cm^3. A reference volume was run with each group of samples, and the standard was rotated among the cells. Constant volumes were sampled using a syringe with a volume of 8.60 cm^3, and this method was occasionally used for soft sediment. Measurements of the cubic sample dimensions were made for well-lithified sediment. Cubes were cut using the double-bladed saw, and individual sample dimensions were measured using the LVDT on the Hamilton Frame

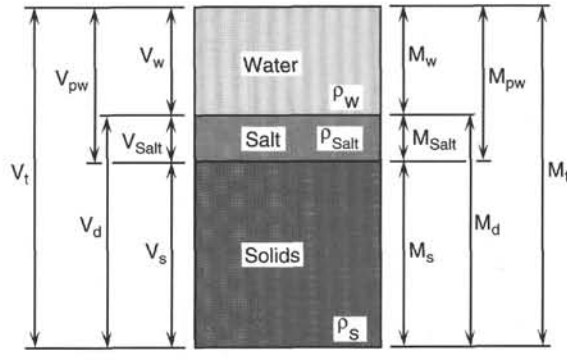

Figure 20. Schematic drawing of the relation between water, salt, and solid components of sediments. Key to abbreviations: V_t = total wet volume of sample, V_{pw} = volume of pore water, V_d = volume of oven-dried sample, V_w = volume of pure water evaporated during oven drying, V_{salt} = volume of salt precipitated during oven drying, V_s = mass of solid particles (mineral grains), ρ_w = pure water density, ρ_{salt} = salt density, ρ_s = density of solids (grain density), M_t = total wet mass of sample, M_{pw} = mass of pore water, M_d = mass of oven-dried sample, M_w = mass of pure water evaporated during oven drying, M_{salt} = mass of salt precipitated during oven drying, M_s = mass of solid particles (mineral grains).

Velocimeter (see below). The dry volume of all samples was determined in the pycnometer.

The tare beakers used for discrete index property determinations were checked for mass and volume prior to the leg. This recalibration

Table 5. Formulas for index properties calculations.

Index properties	Units	Formulas for nonsaline waters	Formulas corrected for saline waters
Water content relative to total wet mass (w_t)	1	$w_t = M_{pw}/M_t$	$w_t = (M_t - M_d) \cdot (1 + s)/M_t$
Water content relative to total wet mass (W_t)	%	$W_t = w_t \cdot 100$	$W_t = w_t \cdot 100$
Water content relative to mass of solids (w_s)	1	$w_s = M_{pw}/M_s$	$w_s = (M_t - M_d)/(M_d - [s \cdot M_t])$
Water content relative to mass of solids (W_s)	%	$W_s = w_s \cdot 100$	$W_s = w_s \cdot 100$
Bulk density (ρ)	g/cm^3	$\rho = M_t/V_t$	$\rho = M_t/V_t$
Density of solids-grain density (ρ_s)	g/cm^3	$\rho_s = M_s/V_s$	$\rho_s = (M_d - M_{Salt})/(V_d - [M_{Salt}/\rho_{Salt}])$
Specific gravity (G_s)	1	$G_s = \rho_s/\rho_w$	$G_s = \rho/(\rho_{pw} - w_s \cdot [\rho - \rho_{pw}])$
Dry density (ρ_d)	g/cm^3	$\rho_d = M_s/V_t$	$\rho_d = (\phi/W_s) \cdot \rho_{pw}$
Porosity (η)	1	$\eta = V_w/V_t$	$\eta = (w_s \cdot \rho)/([1 + w_s] \cdot \rho_{pw})$
Porosity (ϕ)	%	$\phi = \eta \cdot 100$	$\phi = \eta \cdot 100$
Void ratio (e)	1	$e = V_w/V_s$	$e = (w_s \cdot \rho_s)/\rho_{pw}$

was done using the known density of the beakers and determining the mass of each beaker with the Scitech balance. The ODP physical properties data base was updated with these corrected values.

Samples of approximately 10 to 15 cm^3 were taken at least three times per full core for determination of index properties.

Velocimetry

Compressional *P*-wave velocity measurements were obtained by using a Digital Sound Velocimeter (DSV 1) and a Hamilton Frame Velocimeter (DSV 3). In soft sediments *P*-wave velocities were measured by DSV 1 and DSV 3, whereas only DSV 3 was used in lithified sediments.

The velocity is calculated by dividing the distance between a pair of piezoelectric transducers with the traveltime of an acoustic signal between them. DSV 1 is a Dalhousie University/Bedford Institute of Oceanography Digital Sound Velocimeter that contains two transducers separated by approximately 7 cm. The transducers are firmly fixed at one end to a steel plate so that their separation does not change during velocity determinations. They emit 2 µs square waves at about 250 and 750 kHz. The distance between the transducers was evaluated by running a calibration procedure in distilled water. DSV 3 has two transducers; one is fixed in one position, the other is adjustable. The distance between them is measured by a pair of Linear Variable Displacement Transducers (LVDT), and a signal frequency of 500 kHz is emitted. Delays for the transducers were estimated by linear regression of traveltime vs. distance for series of aluminum and lucite standards. Both DSV 1 and DSV 3 are operated from a dedicated microcomputer, which controls all functions of the velocimeters. The transmitted and received signals are digitized by a Nicolet 320 digital oscilloscope and transferred to the microcomputer for further processing. The software selects the first arrival (although manual selection is also available) and calculates the sediment velocity; the full waveform is stored for later calculation of attenuation.

In soft sediments measurements were made directly on the split core, and the *P*-wave velocity was determined in the vertical direction (along the core axis) by DSV 1 and in the horizontal direction (perpendicular to the core axis and through the core liner) by DSV 3. In hard sediments, where induration made it difficult to insert the DSV 1 transducers, samples were cut carefully using a double bladed diamond saw, and the sample thickness was measured directly from the LVDT. Only coherent core pieces that can be cut into cubes are selected for measurements. Therefore there is a bias in the results of this method, as the magnitude of the downhole velocity variation in the data may be overestimated compared to the in situ downhole velocities. In the cube samples the *P*-wave velocity was measured by the DSV 3 in three directions (one vertical and two horizontal). This approach then provides a measure of the acoustic anisotropy (A) within the sediments using the following (Carlson and Christensen, 1977):

$$A = 2 \cdot \frac{V_h - V_v}{V_h + V_v} \tag{6}$$

where V_h = horizontal velocity, and V_v = vertical velocity. A is unitless.

All measurements were made close to where the samples for index property measurements were taken. Filtered seawater was used to improve the acoustic contact between the sample and the transducers.

All velocity data reported here are corrected for in situ temperature and pressure using the following (Wyllie et al., 1956):

$$\frac{1}{V_{corr}} = \frac{1}{V_{meas}} + \eta \cdot \left(\frac{1}{V_{in\ situ}} - \frac{1}{V_{lab}} \right) \tag{7}$$

where V_{corr} = corrected velocity, V_{meas} = measured velocity, η = sediment porosity, $V_{in\ situ}$ = the calculated velocity of seawater at in situ temperature and pressure (using Wilson, 1960), and V_{lab} = the calculated velocity of seawater at the laboratory temperature and pressure (using Wilson, 1960). Units of $1/V_{corr}$ are s/m.

Undrained Shear Strength

The undrained shear strength (S_u) of the sediment was determined using the ODP motorized miniature vane shear device following the procedures of Boyce (1976). Measurements were made using the pocket penetrometer in sediments where progressive cracking occurred prior to failure or where they were too stiff to insert the shear device.

The vane shear instrument measures the difference in rotational strain between the top and bottom of the linear spring using a digital shaft encoder. In the analyses of vane tests, the assumption is made that a cylinder of sediment is uniformly sheared about the axis of the vane in undrained conditions, with cohesion as the principal contributor to shear strength. Departures from this assumption include progressive cracking within and outside of the failing specimen, uplift of the failing core cylinder, drainage of local pore pressures (i.e., the test can no longer be considered to be undrained), and stick-slip behavior.

The vane rotation rate was set to 89°/m. The vanes used for all measurements have a 1:1 blade ratio width with a height of 1.27 cm. The rotational strains are used to compute torque and strain and are recorded on a dedicated microcomputer. The shear strength reported is the peak strength determined from the torque vs. strain plot. In addition to the peak shear strength, the residual strength was determined from the same plot where the failure was not dominated by cracking of the sample (Pyle, 1984).

A pocket penetrometer was used in stiffer sediments. The pocket penetrometer is a small, flat-footed cylindrical probe that is pushed

into the split core to a depth of 6.4 mm. The resulting resistance is the unconfined compressive strength or $2S_u$. A scale directly reads out in units of kg/cm^2. The values of unconfined compression were converted to values of S_u and reported in units of kPa.

Measurements of S_u were only made in soft to very stiff fine-grained sediments, in which all measurements were made close to where the index properties and *P*-wave velocity measurements were performed.

Electrical Resistivity

Electrical resistivity measurements are used to determine formation factor and to estimate porosity. A four-electrode configuration (Wenner spread) with two current and two potential electrodes was used to determine electrical resistivity with a Wayne Kerr Precision Component Analyzer 6425. The device applies a 5-volt alternating square wave across the outer electrodes and measures the potential drop (mV) between the two inner electrodes with a 1.5-mm spacing. It may be used in very stiff sediment since the probe size is small. The potential drop of the sediments was measured by pushing the probe approximately 2 mm into the split core surface. The potential drop is converted to resistance by dividing by the applied current. The electrical resistivity is calculated by multiplying the resistance with the cell constant, which is defined as the cross sectional area divided by the length between the two voltage electrodes. This cell constant was determined for each probe by measuring the resistance of a known fluid (seawater) at controlled temperatures.

Formation factor (F) is the ratio between the resistivity of the saturated sediment and the resistivity of the pore fluid. Porosity (η) of the sediment was estimated from the formation factor following a modified Archie equation (Lovell, 1985) as follows:

$$F = a \cdot \eta^{-m} \quad (8)$$

where a and m are coefficients that vary with sediment type. Measurements were made with the probes aligned perpendicular and parallel to the core axis, and they were made close to those of index properties and *P*-wave velocity. F is unitless.

DOWNHOLE MEASUREMENTS

Introduction

The Lamont-Doherty Earth Observatory's Borehole Research Group (LDEO-BRG) in conjunction with Schlumberger Well Logging Services provides the geophysical well logging aboard the *JOIDES Resolution.* Designed for use in hydrocarbon exploration, the logging tools have been adapted to meet ODP requirements, primarily the reduction of tool diameter to allow insertion into the 3.8-in. drill-string bore.

Downhole logs are used to characterize the geophysical, geochemical, and structural properties of a drilled sequence. Log data offer advantages over core-based analyses in that they are rapidly collected and represent continuous, in situ measurements of the formation. Combined core-log research efforts can potentially integrate the ground-truth information provided by detailed core analyses with continuous and multivariate log data, resulting in continuous and quantitative records of sediment lithologic variability.

After coring is completed, the hole is flushed of debris and a combination of sensors is lowered downhole on a 7-conductor cable. A wireline heave motion compensator is employed during rough seas to minimize the effect of ship heave on the tool position in the borehole. The sensors continuously monitor geophysical, geochemical, or structural properties of the formation, which are recorded typically at 15-cm depth increments by the Schlumberger MAXIS 500, or Cyber Service Unit (CSU) computers. The in-formation depths of investigation and vertical resolutions are sensor-dependent, but are typically between 50 and 100 cm and are summarized in Table 6.

Logging Tool Strings

Four different Schlumberger tool strings were used on Leg 159: (1) a seismic stratigraphic tool string, (2) a lithoporosity tool string, (3) the Formation MicroScanner (FMS), and (4) the geochemical logging tool string (GLT). A schematic diagram of these tool strings is shown in Figure 21.

The seismic stratigraphic and lithoporosity strings frequently are combined to form the Quad combination tool string. Composed of the natural gamma spectrometry tool (NGT), the long spaced sonic tool (LSS/SDT), the phasor dual induction tool (DIT), the dual porosity compensated neutron tool (CNT-G) and the high-temperature lithodensity tool (HLDT), this tool string reaches a length of 33 m, making it difficult or impractical to run in short holes. Splitting the Quad combination into two separate strings (1 and 2 above) also improves the quality of the sonic and neutron porosity logs. The sonic tool in the seismic stratigraphic tool string requires a centralizer for optimum performance, whereas the neutron porosity and density tools in the lithoporosity tool string perform best when eccentralized in the borehole.

The GLT consists of the gamma-ray spectroscopy tool (GST), the aluminum activation clay tool (AACT), and the NGT. The FMS sonde also includes the general purpose inclinometry cartridge (GPIT) and NGT. The NGT, included at the top of all tool strings, facilitates correlation between logging runs at each logged hole. The Lamont-Doherty temperature logging tool (TLT) was attached to the base of each tool string (excluding the FMS tool string) to monitor borehole temperature variations.

Table 6. Approximate vertical resolution of various logging tools used during Leg 159.

Tool	Vertical resolution	Depth of investigation*
Phasor induction tool (DIT)		
ILD deep resistivity	200 cm	150 cm
ILM medium resistivity	150 cm	76 cm
SFL shallow focused	76 cm	38 cm
Natural gamma-ray spectrometry tool (NGT)	46 cm	Variable (15–30 cm)
Litho-density tool (HLDT)		
Density, photoelectric effect	49 cm	Variable (15–60 cm)
Long Spaced Sonic (LSS)/Sonic Digital Tool (SDT)	61 cm	Variable (10–60 cm)
Gamma-ray spectrometry tool (GST)	75–130 cm	Variable (12–20cm)
Aluminum activation tool (AACT)	25 cm	Variable (12–20 cm)
Dual porosity compensated neutron tool (CNT-G)	55 cm (6-in. sample)	Variable and porosity dependent (15–60 cm)
Formation MicroScanner (FMS)	6 mm	5–25 cm
Lamont temperature tool	(a) 1 fast-response (1 s time constant) reading/s (b) slow-response, high-accuracy reading (10 s time constant) /10 s; vertical resolution depends on logging speed.	

Notes: Standard sampling is at 15-cm (6-in.) intervals. High-resolution sampling is at 5.5-cm (2-in.) intervals. APLPHA processing is a special high-resolution processing routine.
*Depth of investigation is formation and environment specific; these depths are only rough estimates/ranges.

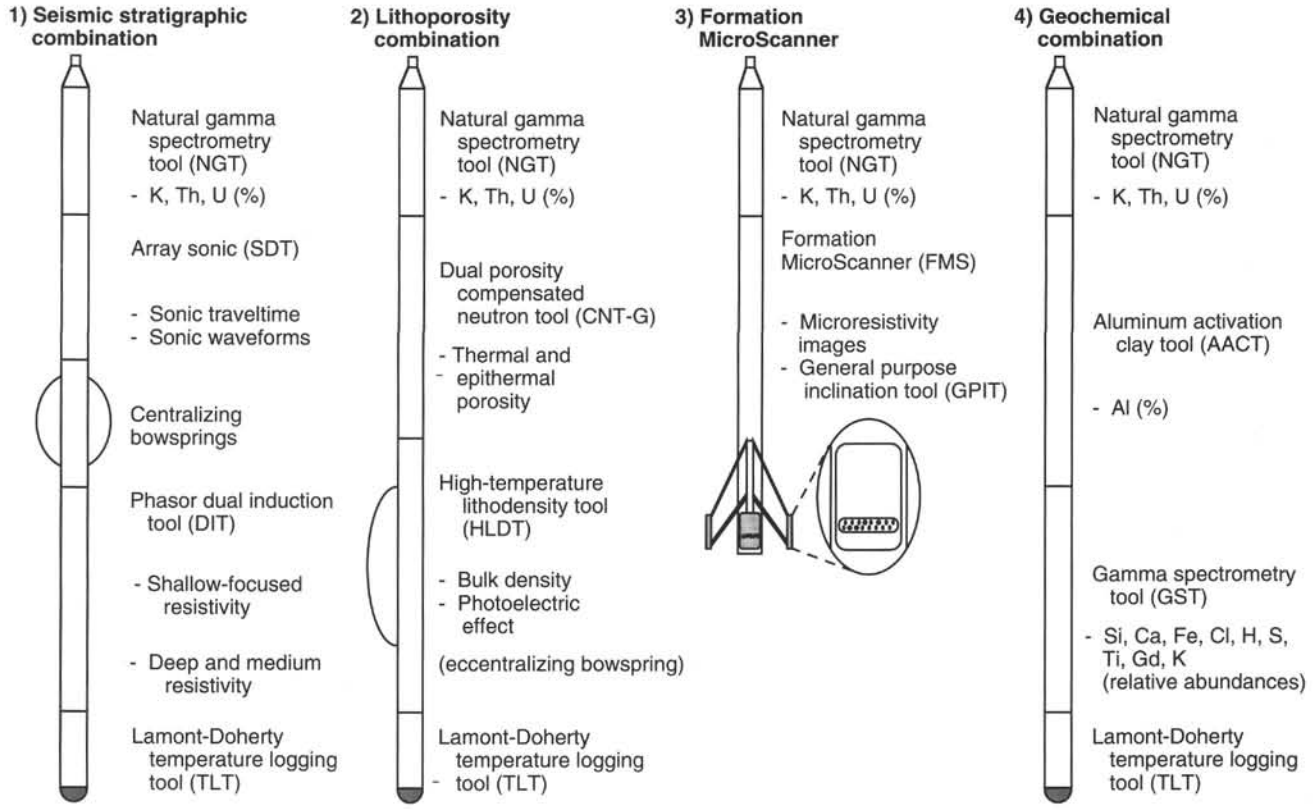

Figure 21. Summary diagram showing the logging tool strings deployed during Leg 159. Tool strings are not drawn to scale.

A brief description of the logging tools employed during Leg 159 is given below. Additional information may be found on the back-pocket CD-ROM, which contains all of the logging data collected during Leg 159. The detailed principles of operation of the various logging sensors can be found in Ellis (1987), Schlumberger (1989), Serra (1984), and Timur and Toksöz (1985).

Electrical Resistivity–Dual Induction Tool

The DIT provides three different measurements of electrical resistivity, each with a different depth of investigation in the formation. Two induction devices (deep and medium resistivity) transmit high-frequency alternating currents through transmitter coils, creating magnetic fields that induce secondary (Foucault) currents in the formation (Ellis, 1987). These ground-loop currents produce new inductive signals, proportional to the conductivity of the formation, which are measured by the receiving coils. The measured conductivities are then converted to resistivity. A third device, a spherically focused resistivity instrument, giving higher vertical resolution, measures the current necessary to maintain a constant voltage drop across a fixed interval.

Water content and salinity are the most significant factors controlling the electrical resistivity of rocks. To a first order, resistivity is related to the inverse square root of porosity (Archie, 1942). Other factors also influencing resistivity include the concentration of hydrous and metallic minerals and the abundance and geometry (tortuosity) of interconnected pore spaces.

High-temperature Lithodensity Tool

The HLDT uses a cesium-137 (^{137}Cs) source of 662 keV gamma rays to measure formation bulk density. The source is mounted in the tool body and an eccentralizing arm presses it and a pair of detectors against the borehole wall. Determination of density is based on the theory of Compton scattering of gamma rays within the formation, which is a function of electron density. The electron density is converted to bulk density on the assumption that most rock-forming elements have atomic weights that are twice their atomic numbers. In addition, the lithodensity tool records a photoelectric effect index. Photoelectric absorption occurs in the energy window below 100 keV and is principally dependent upon the energy of the incident gamma ray and the atomic cross section. The measurement is independent of porosity and therefore can be used as a matrix lithology indicator. The density and photoelectric effect measurements require good contact between the sensor and borehole wall; the tool measures the standoff and corrections can be made for excessive borehole roughness. The intrinsic vertical resolution of the tool is approximately 0.4 m.

The Array–Sonic Digital Tool (Array/SDT)

Sonic tools provide a direct measure of vertical traveltime of sound in the adjacent formation (the interval traveltime or Δt) which is used to calculate the porosity of the formation and sonic velocity. The sonic velocity and density data together are used to calculate an impedance log. A synthetic seismogram is then produced from the impedance log for comparison with site specific seismic reflection profiles.

The Array/SDT is aimed at maximizing the information obtained from measured sonic waveforms by acquiring a digitized full sonic waveform downhole including compressional, shear, and Stoneley waves.

The tool contains two broadband (5 to 18 kHz) piezoelectric transmitters spaced 2 ft apart and two piezoelectric receivers at 3 ft and 5 ft from the upper transmitter. These receivers are used in conjunction with the two transmitters to make a standard short-spaced 3–5 ft and

5–7 ft depth-derived borehole compensated Δt logs. The tool also has an array of eight wideband piezoelectric receivers spaced 6 in. apart, and with the closest one spaced 8 ft from the upper transmitter. Two of the receivers (1 and 5) can be used for making standard long-spaced 8–10 ft and 10–12 ft depth-derived borehole compensated Δt logs. These eight receivers record the full waveform train present. The array waveforms are processed using the slowness-time coherence technique, which measures the similarity of the eight-wave train by comparing a portion of the waveform in receiver 1 to shifted portions of the other seven waveforms.

Dual Porosity Compensated Neutron Tool

The CNT-G consists of a 16-curie americium-beryllium (AmBe) neutron source and a set of two neutron detectors designed to measure neutrons of two different energies (thermal and epithermal neutrons). The radioactive source emits high-energy neutrons (4 MeV) into the formation, which are scattered and slowed by collisions with other nuclei. When the neutrons reach a low energy level (0.025 eV), they are captured and absorbed by atomic nuclei such as H, Cl, Si, and B. Because neutrons have an atomic mass similar to that of H, most neutron slowing is caused by collisions with H, almost all of which resides in water molecules. Therefore, a change in the number of neutrons detected at a receiver can be related to porosity. As water is present both in pores and as bound water (e.g., in clay minerals), porosities measured in the presence of hydrous minerals are often overestimates of true porosity. This can be alleviated by comparing epithermal and thermal neutron porosities (Ellis, 1987). The accuracy of neutron porosity may be adversely affected by variations in hole size that result in an increased abundance of H from seawater drill fluid.

Geochemical Logging Tool String

The geochemical tool string includes the NGT, the GST, and the AACT (Hertzog et al., 1989). Relative concentrations of Si, Ca, Fe, S, H, and Cl, and wet weight percents of K, U, Th, and Al are determined on board ship. Extensive additional shore-based processing is required to obtain dry weight percentages of the above elements at which stage Gd and Ti are also determined. This processing is performed at Leicester University Borehole Research in England (LUBR) and is explained in more detail below (see "Processing of Leg 159 Geochemical Data").

The NGT measures the natural radioactivity of the formation (Lock and Hoyer, 1971). The majority of natural gamma rays are emitted by ^{40}K and by U and Th isotopes and their daughter products. Near-field (i.e., near the borehole wall) natural gamma-ray emissions of the formation are measured by an NaI scintillation detector mounted inside the sonde. The energy spectrum measured by the detector is divided into five discrete energy windows. At each 15-cm sample interval, the total counts recorded in each window are processed to give elemental abundances of K, U, and Th. The in-formation depth of investigation is about 0.3–0.5 m. The NGT is positioned at the top of the tool string measuring the natural radioactivity before the formation is irradiated by the sources in the tools below.

K, U, and Th are generally most abundant in clay minerals, so the gamma-ray log is commonly used as an estimate of the clay content of the formation. Silicic volcaniclastic material and K-feldspar-rich rocks also can have high concentrations of these three elements, so interpretations must be tied to the core lithology. At some sites, the U log closely follows variations in organic carbon content.

The aluminum activation clay tool (AACT) forms the second part of the geochemical tool string measuring the concentration of Al in the formation by delayed neutron activation (Scott and Smith, 1973). When the natural isotope ^{27}Al absorbs a thermal neutron derived from the 2.5 MeV ^{252}Cf source of the AACT, it forms an unstable ^{28}Al atom with a half-life of about 2 min. When the unstable nucleus decays (to ^{28}Si), a gamma ray with a characteristic energy (1779 keV) is emitted and subsequently detected by the AACT. Because the AACT simultaneously counts the natural gamma-ray radiation of the formation, the net Al spectrum is determined by subtracting the count rates from the NGT, which is positioned above the AACT in the tool string.

The gamma-ray spectrometry tool (GST) consists of a pulsed 14 MeV neutron generator and a NaI scintillation detector. Incident neutrons lose energy through inelastic scattering interactions and, on reaching thermal energy levels, are captured by elemental nuclei. Characteristic gamma rays are emitted upon neutron capture; these gamma rays and their relative energy levels are recorded by the tool. The 256-channel energy spectrum is deconvolved to determine relative abundances of Ca, Si, Fe, Cl, H, and S on board ship. The post-cruise processing of the GST data provides the additional elemental yields of Gd and Ti. The above yields (except Cl and H) are then combined with elements determined from the NGT and AACT to derive the dry weight percentages of the elements Si, Ca, Fe, S, Ti, K, Al, in addition to Gd, Th, and U in ppm. If the data quality are sufficiently high, an estimate of (Mg + Na) can be made by using the photoelectric factor from the HLDT.

Formation MicroScanner

The FMS tool produces high-resolution micro-resistivity images of the borehole wall that can be used for detailed sedimentological or structural interpretations. The tool consists of 16 electrodes, or "buttons," on each of four orthogonal pads. These four pads are pressed against the borehole wall. Pad electrodes are spaced about 2.5 mm apart and are arranged in two diagonally offset rows of eight electrodes each (Fig. 21). A focused electrical current flows between buttons and is recorded as a series of curves that reflect the micro-resistivity variations of the formation. Processing converts the measurements into spatially oriented images of the borehole wall using information from the GPIT. Further processing can provide oriented measurements of strike and dip of planar features. The vertical resolution of the FMS is about 6 mm. Coverage is restricted to about 22% of the borehole wall for each pass of the tool. Use of the FMS is restricted to hole diameters less than 37 cm. Thus, little useful information can be obtained from washed-out hole sections.

FMS images may be used in the detailed correlation of core-logging depths, in the orientation of cores, mapping of fractures, faults, foliations and formation structures, as well as determining strikes and dips of bedding (Serra, 1989). The FMS can also provide information on the orientation of the in situ stress field, by imaging the directions of borehole breakouts. In an isotropic, linearly elastic rock subjected to an anisotropic stress field, breakouts form in relation with principal horizontal stresses. Bell and Gough (1979) and Zoback et al. (1988) demonstrated that the stress orientations deduced from such rock breakouts are consistent with other independent stress indicators. The FMS also uses a triaxial magnetometer and accelerometer in the GPIT cartridge. This is primarily used for tool orientation but is useful in determining the hole azimuth and deviation from vertical, often enabling the orientation of core material.

Lamont-Doherty Temperature Logging Tool

The TLT is a self-contained temperature recording tool that can be attached to any Schlumberger tool string. Data from two thermistors and a pressure transducer are collected at a pre-determined rate of one sample per 0.5 to 5.0 s and stored within the tool. Following the logging run, data are transferred from the tool to a shipboard computer for analysis. A fast-response, lower accuracy thermistor is able to detect sudden temperature excursions caused by fluid flow from the formation. A slow-response, higher accuracy thermistor can be used to estimate borehole fluid temperature. If the history of drill-fluid circulation in the hole and at least two temperature logs are available (Jae-

ger, 1961), the post-drilling equilibrium geotherm can be estimated. Conversion to depth is based on pressure recordings from the pressure transducer and from the Schlumberger unit elapsed time (ETIM) records.

Log Data Quality

Log data quality may be seriously degraded by rapid changes in the hole diameter and in sections where the borehole diameter is greatly increased or washed out. The resulting increase in the fluid volume between the formation and the logging tool can also impair data quality. Deep investigation devices such as resistivity and velocity tools are least sensitive to such borehole effects. Nuclear measurements (density, neutron porosity, and both natural and induced spectral gamma ray) are more sensitive due to their shallower depth of investigation and because of the effect of increased drill fluid volume on neutron and gamma-ray attenuation. Corrections can be applied to the original data to reduce these effects. Very large washouts, however, cannot be corrected for.

By use of the NGT on each string, data can be depth correlated between logging runs. Logs from different tool strings may still, however, have minor depth mismatches caused either by cable stretch or ship heave during recording. Small errors in depth matching can impair the multilog analyses in zones of rapidly varying lithology. Ship heave is minimized by a hydraulic wireline heave compensator designed to adjust for rig motion during logging operations. Precise depth matching of logs with cores is difficult in zones where core recovery is low because of the inherent ambiguity of placing the recovered section within the cored interval.

Synthetic Seismograms

Synthetic seismograms are generated from an impedance log. The interval transit time log (from the LSS/SDT) and density log (from the HLDT) are used to generate an impedance log (Gal'perin, 1974). The impedance vs. depth logs are then converted to impedance vs. two-way traveltime and convolved with a zero-phase Ricker wavelet and various other digitalized wavelet samples acquired from the *JOIDES Resolution* seismic source. The dominant frequency of the wavelet is varied depending on the source used in the original seismic profile. The vertical resolution of a 30-Hz wavelet is about 15–30 m (depending on interval velocity), so reflectors cannot generally be attributed to smaller-scale lithologic intervals (less than 30 m). The final synthetic seismogram calculated includes interbed multiples.

Shore-based Log Processing

Additional log processing and display have been performed at each of the four sites by the Borehole Research Group (BRG) at LDEO, Institut Méditerranéen de Technologie (IMT), and Leicester University, using Schlumberger "Logos" software and additional programs developed by members of the BRG. Displays of most of these processed data appear with accompanying text at the end of the appropriate site chapters in this volume. Files of all processed logs (including FMS, dipmeter, BRG temperature, high-resolution density and neutron data), sonic waveforms, and explanatory text are included on the CD-ROM (back pocket); a directory of the contents of the CD is found at the front of this volume.

Shore-based processing of conventional logging data from each hole includes (1) depth adjustments of all logs to a common measurement below the seafloor; (2) corrections specific to certain tools; and (3) quality control and rejection of unrealistic values.

The depth-shifting procedure is based on an interactive, graphical depth-match program that allows the processor to visually correlate logs and define appropriate shifts. The reference log and the log to be adjusted in depth are displayed side-by-side on a screen, and vectors connect the two at positions chosen by the user. The total gamma-ray curve (SGR) from the NGT tool run on each logging string was used in most cases to correlate the logging runs. In general, the reference curve is chosen on the basis of constant, low cable tension and high cable speed (tools run at faster speeds are less likely to stick and are less susceptible to data degradation caused by ship heave). Other factors, however, such as the length of the logged interval, the presence of drill pipe, and the statistical quality of the collected data (better statistics are obtained at lower logging speeds) are also considered in the selection. A list of the amount of differential depth shifts applied at each hole is available upon request to BRG (LDEO).

Specific tool corrections are performed on the gamma-ray data to account for changes in borehole size and for the composition of the drilling fluid. Processing techniques unique to the ACT and GST tools of the geochemical string are described in detail below.

In addition to the standard 15.24-cm sampling rate, bulk density and neutron porosity data were recorded at a sampling rate of 2.54 and 5.08 cm, respectively. The enhanced bulk density curve is the result of a Schlumberger enhanced processing technique performed on the MAXIS system on board. In normal processing, short-spacing data are smoothed to match the long-spacing data; in enhanced processing, this is reversed. Where there is good contact between the HLDT pad and the borehole wall (low density correction) the results are improved, because the short-spacing data have better vertical resolution.

Quality control has been performed by cross-correlation of all logging data. If the data processor concludes that individual log measurements represent unrealistic values, the choices are either to discard the data outright and substitute the null value of "–999.25," or identify a specific depth interval containing suspect values that must be used with caution. The latter are noted in the text that accompanies all processed log displays. Quality control of the acoustic data is based on discarding any of the four independent transit time measurements that were negative or that fell outside a range of reasonable values selected by the processor.

Locally, some intervals of log data appear unreliable (usually because of poor hole conditions) and are not processed. In general, a large (>12 in.) and/or irregular borehole affects most recordings, particularly those that require eccentralization (CNT-G, HLDT) and a good contact with the borehole wall. Hole deviation also can degrade the data; the FMS, for example, is not designed to be run in holes that are more than 10° off vertical, as the tool weight might cause the caliper to close.

PROCESSING OF LEG 159 GEOCHEMICAL DATA[3]

Geochemical Tool String

The geochemical logging tool string (GLT*) consists of four separate logging tools: the natural gamma spectrometry tool (NGT), the compensated neutron tool (CNT*), the aluminum activation clay tool (AACT*), and the gamma-ray spectrometry tool (GST*). A schematic drawing of the GLT, which was run in Hole 959D on Leg 159, is shown in Figure 22. These four tools use three separate modes of gamma-ray spectroscopy for a comprehensive elemental analysis of the formation. The NGT is located at the top of the tool string so that it can measure the naturally occurring radionuclides, thorium (Th), uranium (U), and potassium (K), before the formation is irradiated by the nuclear sources contained in the lower tools (Fig. 22). The CNT, located below the NGT, carries a californium (^{252}Cf) neutron source to activate the Al atoms in the formation. The AACT, a modified NGT, is located below the ^{252}Cf source, measuring the activated gamma rays in the formation. By combining the AACT measurement

[3]James F. Bristow, Lee Ewert, and Peter K. Harvey, Borehole Research, Department of Geology, University of Leicester, Leicester, LE1 7RH, United Kingdom.

*Trademark of Schlumberger.

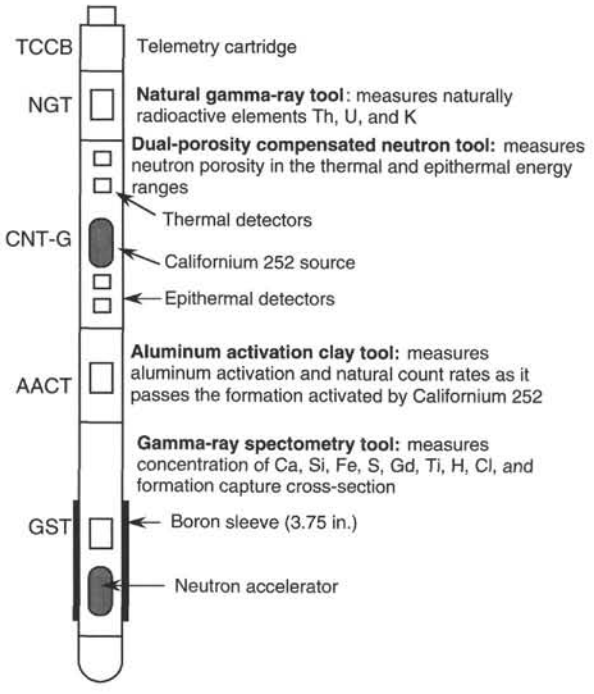

Figure 22. Schematic drawing of the Schlumberger geochemical logging tool string used by the Ocean Drilling Program.

with the previous NGT measurement, the background radiation is subtracted and a reading of formation Al is obtained (Scott and Smith, 1973). The GST, at the base of the string, carries a pulsed neutron generator to induce prompt-capture gamma-ray reactions in the borehole and formation and an NaI(Tl) scintillation detector to measure the energy spectrum of gamma rays generated by the prompt neutron capture reactions. As each of the elements in the formation is characterized by a unique spectral signature, it is possible to derive the contribution (or yield) of each of the major elements silicon (Si), iron (Fe), calcium (Ca), titanium (Ti), sulfur (S), gadolinium (Gd), and potassium (K) from the measured spectrum and, in turn, to estimate the relative abundance of each in the formation when combined with the elemental concentrations from the NGT and AACT (Hertzog et al., 1989). The GST also measures the hydrogen (H) and chlorine (Cl) in the borehole and formation, although these elements are not directly used for determining the rock geochemistry.

The only major rock-forming elements not measured by the geochemical tool string are magnesium (Mg) and sodium (Na); the neutron-capture cross sections of these elements are too small relative to their typical abundances for the GLT to detect. A rough estimate of Mg + Na can be made in some instances by using the photoelectric factor (PEF), measured by the lithodensity tool (Hertzog et al., 1989). This calculation was not implemented on the geochemical data from Hole 959D as the (Mg + Na) component was generally below the detection resolution of this technique (Pratson et al., 1993).

Data Reduction

The well-log data from the Schlumberger tools are transmitted digitally up a wireline and are recorded and processed on the *JOIDES Resolution* in the Schlumberger Cyber Service Unit (CSU). The results from the CSU are made available as "field logs" for initial shipboard interpretation. Subsequent reprocessing is necessary to correct the data for the effects of fluids added to the well, logging speed, and drill-pipe interference. Processing of the spectrometry data is required to transform the relative elemental yields into oxide weight fractions.

The processing is performed with a set of log-interpretation programs written by Schlumberger but have been slightly modified to account for the lithologies and hole conditions encountered in ODP holes. The processing steps are summarized below.

Step 1: Reconstruction of relative elemental yields from recorded spectral data

This first processing step compares the measured spectra from the GST with a series of "standard" spectra to determine the relative contribution (or yield) of each element. These "standards" approximate the spectrum of each element. Using a weighted, least-squares inversion method, the relative elemental yields are calculated at each depth level.

Six elemental standards (Si, Fe, Ca, S, Cl, and H) are used to produce the shipboard yields, but three additional standards (Ti, Gd, and K) can be included in the post-cruise processing to improve the fit of the spectral standards to the measured spectra (Grau and Schweitzer, 1989). The ability to detect an element is principally dependent on the size of its capture cross section and its abundance in the formation. Although Ti, Gd, and K often appear in the formation in very low concentrations, they can make a significant contribution to the measured spectra because they have large neutron-capture cross sections. Gd, for example, has a capture cross section of 49,000 barns, whereas that of Si is 0.16 barns (Hertzog et al., 1989). Therefore, including Gd is necessary when calculating the best fit of the standard spectra to the measured spectrum, even though its typical concentration is only a few parts per million.

The elemental standards (Si, Ca, Fe, Ti, Gd, S, Cl, and H) were used in the spectral analysis step for Hole 959D. The spectral standard for K was not used in the final analysis because its inclusion in the spectral inversion was found to increase the noise level in the other elemental yields. A linear 10-point (5 ft, 1.52 m) moving average was applied to the output elemental yields to increase the signal to noise ratios.

Step 2: Depth-shifting

Geochemical processing involves the integration of data from the different tool strings; consequently, it is important that all the data are depth-correlated to one reference logging run. The NGT, run on each of the logging tool strings, provides a spectral gamma-ray curve with which to correlate each of the logging runs. A reference run is chosen on the basis of constant and low cable tension, and high cable speed (tools run at faster speeds are less likely to stick and are less susceptible to data degradation caused by ship heave). The depth-shifting procedure involves picking a number of reference points based on similar log character and then invoking a program that expands and compresses the matching logging run to fit the reference logging run. The main (lower) run of the Quad combination tool string was chosen as the reference run for Hole 959D.

Step 3: Calculation of total radioactivity and Th, U, and K concentrations

The third processing routine calculates the total natural gamma-ray radiation in the formation, as well as concentrations of Th, U, and K, using the counts in five spectral windows from the NGT (Lock and Hoyer, 1971). This routine resembles shipboard processing; however, the results are improved during post-cruise processing by including corrections for hole-size changes and temperature variations. A Kalman filtering (Ruckebusch, 1983) is used in the CSU processing at sea to minimize the statistical uncertainties in the logs, which can otherwise create erroneous negative values and anti-correlation (es-

pecially between Th and U). An alpha filter has been introduced more recently and is now recommended by Schlumberger for shore-based processing. This filter strongly smooths the raw spectral counts but keeps the total gamma-ray curve unsmoothed before calculating out the Th, U, and K. The outputs of this program are K (wet wt%), U (ppm), and Th (ppm), as well as total gamma ray and computed gamma ray (total gamma ray minus U contribution). They are displayed as a function of depth in the log summary figures at the end of the relevant site chapter.

Step 4: Calculation of Al concentration

The fourth processing routine (PREACT) calculates the concentration of Al in the formation using recorded gamma-ray data from four energy windows on the AACT. During this step, corrections are made for natural radioactivity, borehole-fluid neutron-capture cross section, formation neutron-capture cross section, formation slowing-down length, and borehole size.

Porosity and density logs are needed as inputs into this routine to convert the wet-weight percentages of K and Al curves to dry-weight percentages. To derive the best porosity log, shipboard core porosity measurements were compared with porosity logs calculated from the resistivity (using the relationship of Archie, 1942) and bulk density logs, and taken from the neutron porosity tool. The best porosity log was derived by a splice of the resistivity porosity (530 to 744 mbsf) and the neutron porosity (744 to 930 mbsf). The bulk density log used as input into PREACT was edited to remove extreme low values caused by borehole washouts over the intervals 796–809 and 867–873 mbsf.

A correction is also made for Si interference with Al the ^{252}Cf source activates the Si, producing the aluminum isotope, ^{28}Al, (Hertzog et al., 1989). The program uses the Si yield from the GST to determine the Si background correction. The program outputs dry-weight percentages of Al and K, which are combined in the next processing step with the GST-derived elemental yields in the oxide closure model.

Step 5: Normalization of elemental yields from the GST to calculate the elemental weight fractions

Relative concentrations of the GST-derived elemental yields can be determined by dividing each elemental yield by a relative spectral sensitivity factor (S_i). This factor is principally related to the thermal neutron-capture cross sections and also to its gamma-ray production and detection probability of each element (Hertzog et al., 1989). The relative elemental concentrations are related to the desired absolute concentrations by a depth-dependent normalization factor (F), as defined by the relationship:

$$Wt_i = FY_i / S_i \tag{9}$$

where Wt_i = absolute elemental concentration, and Y_i = relative elemental yield.

The normalization factor is calculated on the basis that the sum of all the elemental weight fractions is unity (100%). The closure model handles the absence of carbon and oxygen, which are not measured by this tool string, with the approximation that each of the measurable elements combines with a known oxide or carbonate. The dry weight percentages of Al and K are normalized with the reconstructed elemental yields to determine the normalization factor at each depth interval from the following equation:

$$F(\sum_i X_i Y_i / S_i) + X_k Wt_k + X_{Al} Wt_{Al} = 100, \tag{10}$$

where

Table 7. Oxide factors used in normalizing elements to 100% and converting elements to oxides.

Element	Oxide/carbonate	Conversion factor
Si	SiO_2	2.139
Ca	$CaCO_3$	2.497
Fe	FeO*	1.358
K	K_2O	1.205
Ti	TiO_2	1.668
Al	Al_2O_3	1.889

X_i = oxide factor; atomic weight of the associated oxide or carbonate of element i ÷ atomic weight of element i,
X_k = oxide factor; atomic weight K_2O ÷ atomic weight of K,
Wt_k = dry-weight percentage of K as determined from the NGT,
X_{Al} = oxide factor; atomic weight of Al_2O_3 ÷ atomic weight of Al, and
Wt_{Al} = dry-weight percentage of Al, as determined from the AACT.

The value X_i accounts for the C and O associated with each element. Table 7 lists the oxide factors used in this calculation for Hole 959D.

Step 6: Calculation of oxide percentages

This routine converts the elemental weight percentages into oxide percentages by multiplying each by its associated oxide factor, as shown in Table 7. The results are displayed as a function of depth in the log summary figures at the end of the relevant site chapter.

Step 7: Calculation of error logs

The statistical uncertainty of each element is calculated for each of the elements measured with the GST and NGT (Grau et al., 1990; Schweitzer et al., 1988). This error is strongly related to the normalization factor, which is calculated at each depth level (Eq. 10). The normalization factor is displayed to the right of the logs in the log summary figures at the end of the relevant site chapter. A lower normalization factor represents better counting statistics and therefore higher quality data.

REFERENCES

Archie, G.E., 1942. The electrical resistivity log as an aid in determining some reservoir characteristics. *Trans. Am. Inst. Min. Metall. Pet. Eng.*, 146:54–63.

ASTM, 1989. *Annual Book of ASTM Standards for Soil and Rock: Building Stones* (Vol. 4.08): *Geotextiles:* Philadelphia (Am. Soc. Testing Materials).

Bell, J.S., and Gough, D.I., 1979. Northeast-southwest compressive stress in Alberta: evidence from oil wells. *Earth Planet. Sci. Lett.*, 45:475–482.

Berggren, W.A., Kent, D.V., Swisher, C.C., III, and Aubry, M.-P., in press. A revised Cenozoic geochronology and chronostratigraphy. *In* Berggren, W.A., Kent, D.V., Aubry, M.-P., and Hardenbol, J. (Eds.), *Geochronology, Time Scales, and Global Stratigraphic Correlations: A Unified Temporal Framework for an Historical Geology.* Spec. Publ.—Soc. Econ. Paleontol. Mineral., 54.

Boyce, R.E., 1976. Definitions and laboratory techniques of compressional sound velocity parameters and wet-water content, wet-bulk density, and porosity parameters by gravimetric and gamma-ray attenuation techniques. *In* Schlanger, S.O., Jackson, E.D., et al., *Init. Repts. DSDP*, 33: Washington (U.S. Govt. Printing Office), 931–958.

Brown, G., 1980. Associated minerals. *In* Brindley, G.W., and Brown, G. (Eds.), *Crystal Structures of Clay Minerals and Their X-ray Identification.* Mineral. Soc. Monogr. London, 5:361–410.

Brown, G., and Brindley, G.W., 1980. X-ray diffraction procedures for clay mineral identification. *In* Brindley, G.W., and Brown, G. (Eds.), *Crystal*

Structures of Clay Minerals and Their X-ray Identification. Mineral. Soc. Monogr. London, 5:305–359.

Bukry, D., 1973. Low latitude coccolith biostratigraphic zonation. *In* Edgar, N.T., Saunders, J.B., et al., 1973. *Init. Repts. DSDP,* 15: Washington (U.S. Govt. Printing Office), 685–703.

———, 1975. Coccolith and silicoflagellate stratigraphy, northwestern Pacific Ocean, Deep Sea Drilling Project Leg 32. *In* Larson, R.L., Moberly, R., et al., *Init. Repts. DSDP,* 32: Washington (U.S. Govt. Printing Office), 677–701.

Cande, S.C., and Kent, D.V., 1992. A new geomagnetic polarity time scale for the Late Cretaceous and Cenozoic. *J. Geophys. Res.,* 97:13917–13951.

Carlson, R.L., and Christensen, N.I., 1977. Velocity anisotropy and physical properties of deep-sea sediments from the western South Atlantic. *In* Supko, P.R., Perch-Nielsen, K., et al., *Init. Repts. DSDP,* 39: Washington (U.S. Govt. Printing Office), 555–559.

Caron, M., 1985. Cretaceous planktonic foraminifera. *In* Bolli, H.M., Saunders, J.B., and Perch-Nielsen, K. (Eds.), *Plankton Stratigraphy:* Cambridge (Cambridge Univ. Press), 17–86.

Curry, W.B., Shackleton, N.J., Richter, C., et al., 1995. *Proc. ODP, Init. Repts.,* 154: College Station, TX (Ocean Drilling Program).

Ellis, D.V., 1987. *Well Logging For Earth Scientists:* New York (Elsevier).

Emeis, K.-C., and Kvenvolden, K.A., 1986. Shipboard organic geochemistry on *JOIDES Resolution. ODP Tech. Note,* 7.

Erba, E., Premoli Silva, I., and Watkins, D.K., in press. Cretaceous calcareous plankton biostratigraphy of Sites 872 to 879 (Leg 144). *In* Haggerty, J.A., Premoli Silva, I., Rack, F., and McNutt, M.K. (Eds.), *Proc. ODP, Sci. Results,* 144: College Station, TX (Ocean Drilling Program).

Espitalié, J., Deroo, G., and Marquis, F., 1986. La pyrolyse Rock-Eval et ses applications, Partie III. *Rev. Inst. Fr. Pet.,* 41:73–89.

Gal'perin, E.I., 1974. *Vertical Seismic Profiling.* Spec. Publ.—Soc. Explor. Geophys., 12.

Gartner, S., Jr., 1977. Calcareous nannofossil biostratigraphy and revised zonation of the Pleistocene. *Mar. Micropaleontol.,* 2:1–25.

Gieskes, J.M., Gamo, T., and Brumsack, H., 1991. Chemical methods for interstitial water analysis aboard *JOIDES Resolution. ODP Tech. Note,* 15.

Grau, J.A., and Schweitzer, J.S., 1989. Elemental concentrations from thermal neutron capture gamma-ray spectra in geological formations. *Nucl. Geophys.,* 3:1-9.

Grau J.A., Schweitzer, J.S. and Hertzog, R.C., 1990. Statistical uncertainties of elemental concentrations extracted from neutron-induced gamma-ray measurements. *IEEE Trans. Nuclear Sci.,* 37:2175-2178.

Harland, W.B., Armstrong, R.L., Cox, A.V., Craig, L.E., Smith, A.G., and Smith, D.G., 1990. *A Geologic Time Scale 1989:* Cambridge (Cambridge Univ. Press).

Hertzog, R.C., Colson, J.L., Seeman, B., O'Brien, M.S., Scott, H.D., McKeon, D.C., Wraight, P.D., Grau, J.A., Ellis, D.V., Schweitzer, J.S., and Herron, M.M., 1989. Geochemical logging with spectrometry tools. *SPE Form. Eval.,* 4:153–162.

Hoppie, B.W., Blum, P., and the Shipboard Scientific Party, 1994. Natural gamma-ray measurements on ODP cores: introduction to procedures with examples from Leg 150. *In* Mountain, G.S., Miller, K.G., Blum, P., et al., *Proc. ODP, Init. Repts.,* 150: College Station, TX (Ocean Drilling Program), 51–59.

Jaeger, J.C., 1961. The effect of the drilling fluid on temperatures measured in boreholes. *J. Geophys. Res.,* 66:563–569.

Kvenvolden, K.A., and McDonald, T.J., 1986. Organic geochemistry on the *JOIDES Resolution*–an assay. *ODP Tech. Note,* 6.

Lee, T.-C., 1989. Thermal conductivity measured with a line source between two dissimilar media equals their mean conductivity. *J. Geophys. Res.,* 94:12443–12447.

Lock, G.A., and Hoyer, W.A., 1971. Natural gamma ray spectral logging. *Log Analyst,* 12:3–9.

Lovell, M.A., 1985. Thermal conductivity and permeability assessment by electrical resistivity measurements in marine sediments. *Mar. Geotechnol.,* 6:205–240.

MacLeod, C.J., 1994. Structure of the outer Tonga forearc at Site 841. *In* Hawkins, J., Parson, L., Allan, J., et al., *Proc. ODP, Sci. Results,* 135: College Station, TX (Ocean Drilling Program), 313–329.

MacLeod, C.J., Parson, L.M., and Sager, W.W., 1994. Reorientation of cores using the Formation MicroScanner and Borehole Televiewer: application to structural and paleomagnetic studies with the Ocean Drilling Program. *In* Hawkins, J., Parson, L., Allan, J., et al., *Proc. ODP, Sci. Results,* 135: College Station, TX (Ocean Drilling Program), 301–311.

MacLeod, C.J., Parson, L.M., Sager, W.W., and the ODP Leg 135 Scientific Party, 1992. Identification of tectonic rotations in boreholes by the integration of core information with Formation MicroScanner and Borehole Televiewer images. *In* Hurst, A., Griffiths, C.M., and Worthington, P.F. (Eds.), *Geological Applications of Wireline Logs II.* Geol. Soc. Spec. Publ. London, 65:235–246.

Manheim, F.T., and Sayles, F.L., 1974. Composition and origin of interstitial waters of marine sediments based on deep sea drill cores. *In* Goldberg, E.D. (Ed.), *The Sea* (Vol. 5): New York (Wiley Interscience), 527–568.

Martini, E., 1971. Standard Tertiary and Quaternary calcareous nannoplankton zonation. *In* Farinacci, A. (Ed.), *Proc. 2nd Int. Conf. Planktonic Microfossils Roma:* Rome (Ed. Tecnosci.) 2:739–785.

Mayer, L., Pisias, N., Janecek, T., et al., 1992. *Proc. ODP, Init. Repts.,* 138 (Pts. 1 and 2): College Station, TX (Ocean Drilling Program).

Mazzullo, J.M., Meyer, A., and Kidd, R.B., 1988. New sediment classification scheme for the Ocean Drilling Program. *In* Mazzullo, J., and Graham, A.G., *Handbook for Shipboard Sedimentologists.* ODP Tech. Note, 8:45–67.

Moore, D.M., and Reynolds, R.C., Jr., 1989. *X-ray Diffraction and the Identification and Analysis of Clay Minerals:* Oxford (Oxford Univ. Press).

Munsell Soil Color Charts, 1975: Baltimore (Munsell Color).

Okada, H., and Bukry, D., 1980. Supplementary modification and introduction of code numbers to the low-latitude coccolith biostratigraphic zonation (Bukry, 1973; 1975). *Mar. Micropaleontol.,* 5:321–325.

Perch-Nielsen, K., 1985. Mesozoic calcareous nannofossils. *In* Bolli, H.M., Saunders, J.B., and Perch-Nielsen, K. (Eds.), *Plankton Stratigraphy:* Cambridge (Cambridge Univ. Press), 329–426.

Pratson, E.L., Broglia, C., and Jarrard, R., 1993. Data report: geochemical well logs through Cenozoic and Quaternary sediments from Sites 815, 817, 820, 822, and 823. *In* McKenzie, J.A., Davies, P.J., Palmer-Julson, A., et al., *Proc. ODP, Sci. Results,* 133: College Station, TX (Ocean Drilling Program), 795–817.

Pyle, M.R., 1984. Vane shear data on undrained residual strength. *J. Geotech. Engr. Div., Am. Soc. Civ. Eng.,* 110:543–547.

Ratcliffe, E.H., 1959. Thermal conductivities of fused and crystalline quartz. *Br. J. Appl. Phys.,* 7:276–297.

Rio, D., Sprovieri, R., Thunell, R., Vergnaud Grazzini, C., and Glaçon, G., 1990. Pliocene-Pleistocene paleoenvironmental history of the western Mediterranean; a synthesis of ODP Site 653 results. *In* Kastens, K.A., Mascle, J., Auroux, C., et al., *Proc. ODP, Sci. Results,* 107: College Station, TX (Ocean Drilling Program), 695–704.

Robaszynski, F., Caron, M. (Coord.), and the European Working Group on Planktonic Foraminifera, 1979. *Atlas de Foraminifères Planctoniques du Crétacé Moyen* (Vols. 1 and 2). Cah. Micropaleontol.

Robaszynski, F., Caron, M., Gonzalez-Donoso, J.-M., Wonders, A.A.H., and the European Working Group on Planktonic Foraminifera, 1984. Atlas of Late Cretaceous globotruncanids. *Rev. Micropaleontol.,* 26:145–305.

Roth, P.H., 1978. Cretaceous nannoplankton biostratigraphy and oceanography of the northwestern Atlantic Ocean. *In* Benson, W.E., Sheridan, R.E., et al., *Init. Repts. DSDP,* 44: Washington (U.S. Govt. Printing Office), 731–759.

Ruckebusch, G., 1983. A Kalman filtering approach to natural gamma ray spectroscopy in well logging. *IEEE Trans. Autom. Control,* AC-28:372–380.

Sass, J.H., Kennelly, J.P., Jr., Smith, E.P., and Wendt, W.E., 1984. Laboratory line-source methods for the measurement of thermal conductivity of rocks near room temperature. *Open-File Rep.—U.S. Geol. Surv.,* 84-0091.

Schlumberger, 1989. *Log Interpretation Principles/Applications:* Houston, TX (Schlumberger Educ. Services).

Schweitzer, J.S., Grau, J.A., and Hertzog, R.C., 1988. Precision and accuracy of short-lived activation measurements for in situ geological analyses. *J. Trace Microprobe Techniques,* 6:437–451.

Scott, H.D., and Smith, M.P., 1973. The aluminum activation log. *Log Analyst,* 14:3–12.

Serra, O., 1989. *Formation MicroScanner Image Interpretation:* Houston (Schlumberger Educ. Services).

———, 1984. *Fundamentals of Well Log Interpretation* (Vol. 1): *The Acquisition of Logging Data:* Amsterdam (Elsevier).

Shepard, F., 1954. Nomenclature based on sand-silt-clay ratios. *J. Sediment. Petrol.,* 24:151–158.

Shipboard Scientific Party, 1990. Explanatory notes. *In* Rangin, C., Silver, E.A., von Breymann, M.T., et al., *Proc. ODP, Init. Repts.,* 124: College Station, TX (Ocean Drilling Program), 7–33.

Sissingh, W., 1977. Biostratigraphy of Cretaceous calcareous nannoplankton. *Geol. Mijnbouw,* 56:37–65.

Suess, E., von Huene, R., et al., 1988. *Proc. ODP, Init. Repts.,* 112: College Station, TX (Ocean Drilling Program).

Thierstein, H.R., 1973. Lower Cretaceous calcareous nannoplankton biostratigraphy. *Abh. Geol. Bundesanst. (Austria),* 29:1–52.

————, 1976. Mesozoic calcareous nannoplankton biostratigraphy of marine sediments. *Mar. Micropaleontol.,* 1:325–362.

Timur, A., and Toksöz, M.N., 1985. Downhole geophysical logging. *Annu. Rev. Earth Planet. Sci.,* 13:315–344.

Vacquier, V., 1985. The measurement of thermal conductivity of solids with a transient linear heat source on the plane surface of a poorly conducting body. *Earth Planet. Sci. Lett.,* 74:275–279.

Von Herzen, R.P., and Maxwell, A.E., 1959. The measurement of thermal conductivity of deep-sea sediments by a needle-probe method. *J. Geophys. Res.,* 64:1557–1563.

Wentworth, C.K., 1922. A scale of grade and class terms for clastic sediments. *J. Geol.,* 30:377–392.

Westbrook, G.K., Carson, B., Musgrave, R.J., et al., 1994. *Proc. ODP, Init. Repts.,* 146 (Pt. 1): College Station, TX (Ocean Drilling Program).

Westphal, M., Bazhenov, M.L., Lauer, J.P., Pechersky, D.M., and Sibuet, J.-C., 1986. Paleomagnetic implications on the evolution of Tethys Belt from the Atlantic Ocean to the Palmirs since the Triassic. *Tectonophysics,* 123:37–82.

Wilson, W.D., 1960. Speed of sound in seawater as a function of temperature, pressure and salinity. *J. Acoust. Soc. Am.,* 32:641–644.

Wyllie, M.R.J., Gregory, A.R., and Gardner, L.W., 1956. Elastic wave velocities in heterogeneous and porous media. *Geophysics,* 21:41–70.

Zijderveld, J.D.A., 1967. AC demagnetization of rocks: analysis of results. *In* Collinson, D.W., Creer, K.M., and Runcorn, S.K. (Eds.), *Methods in Palaeomagnetism:* New York (Elsevier), 254–286.

Zoback, M.D., Zoback, M.L., Mount, V.S., Suppe, J., Eaton, J.P., Healy, J.H., Oppenheimer, D.H., Reasenberg, P.A., Jones, L.M., Raleigh, C.B., Wong, I.G., Scotti, O., and Wentworth, C.M., 1987. New evidence on the state of stress of the San Andreas Fault. *Science,* 238:1105–1111.

Ms 159IR-102